clean technologies

MDPI

Article

High-Temperature Steam- and CO_2-Assisted Gasification of Oil Sludge and Petcoke

Sergey M. Frolov [1,2,*], Viktor A. Smetanyuk [1], Ilyas A. Sadykov [1], Anton S. Silantiev [1,2], Fedor S. Frolov [1], Vera Ya. Popkova [1], Jaroslav K. Hasiak [3], Anastasiya G. Buyanovskaya [3], Rina U. Takazova [3], Tatiana V. Dudareva [1], Valentin G. Bekeshev [1], Alexey B. Vorobyov [1], Alexey V. Inozemtsev [1] and Jaroslav O. Inozemtsev [1]

[1] Semenov Federal Research Center for Chemical Physics of the Russian Academy of Sciences, 4, Kosyging Street, Moscow 119991, Russia; smetanuk@mail.ru (V.A.S.); ilsadykov@mail.ru (I.A.S.); silantevu@mail.ru (A.S.S.); f.frolov@chph.ru (F.S.F.); vera.popkova@chph.ras.ru (V.Y.P.); yanadva@mail.ru (T.V.D.); bvg495@yandex.ru (V.G.B.); vorob1946@bk.ru (A.B.V.); vectr1@yandex.ru (A.V.I.); 79637502482@yandex.ru (J.O.I.)

[2] Kutateladze Institute of Thermophysics, Siberian Branch of the Russian Academy of Sciences, 1, Ac. Lavrentieva Avenue, Novosibirsk 630090, Russia

[3] Nesmeyanov Institute of Organoelement Compounds of the Russian Academy of Sciences, 28 Vavilov Street, Moscow 119443, Russia; hasiak1996@gmail.com (J.K.H.); buyan.an@bk.ru (A.G.B.); rina@ineos.ac.ru (R.U.T.)

* Correspondence: smfrol@chph.ras.ru

Abstract: A new high-temperature allothermal gasification technology is used to process three types of oil waste: ground oil sludge (GOS), tank oil sludge (TOS), and petcoke. The gasifying agent (GA), mainly composed of H_2O and CO_2 at a temperature above 2300 K and atmospheric pressure, is produced by pulsed detonations of a near-stochiometric methane-oxygen mixture. The gasification experiments show that the dry off-gas contains 80–90 vol.% combustible gas composed of 40–45 vol.% CO, 28–33 vol.% H_2, 5–10 vol.% CH_4, and 4–7 vol.% noncondensable C_2–C_3 hydrocarbons. The gasification process is accompanied by the removal of mass from a flow gasifier in the form of fine solid ash particles with a size of about 1 μm. The ash particles have a mesoporous structure with a specific surface area ranging from 3.3 to 15.2 m^2/g and pore sizes ranging from 3 to 50 nm. The measured wall temperatures of the gasifier are in reasonable agreement with the calculated value of the thermodynamic equilibrium temperature of the off-gas. The measured CO content in the off-gas is in good agreement with the thermodynamic calculations. The reduced H_2 content and elevated contents of CH_4, CO_2, and C_xH_y are apparently associated with the nonuniform distribution of the waste/GA mass ratio in the gasifier. To increase the H_2 yield, it is necessary to improve the mixing of waste with the GA. It is proposed to mix crushed petcoke with oil sludge to form a paste and feed the combined waste into the gasifier using a specially designed feeder.

Keywords: high-temperature gasification of organic waste; gas detonation products; oil sludge; petcoke; off-gas; hydrogen

check for updates

Academic Editors: Sabino De Gisi, Constantinos V. Chrysikopoulos and Dmitry Yu. Murzin

Received: 27 September 2024
Revised: 19 November 2024
Accepted: 11 February 2025
Published: 14 February 2025

Citation: Frolov, S.M.; Smetanyuk, V.A.; Sadykov, I.A.; Silantiev, A.S.; Frolov, F.S.; Popkova, V.Y.; Hasiak, J.K.; Buyanovskaya, A.G.; Takazova, R.U.; Dudareva, T.V.; et al. High-Temperature Steam- and CO_2-Assisted Gasification of Oil Sludge and Petcoke. *Clean Technol.* **2025**, *7*, 17. https://doi.org/10.3390/cleantechnol7010017

Copyright: © 2025 by the authors. Licensee MDPI, Basel, Switzerland. This article is an open access article distributed under the terms and conditions of the Creative Commons Attribution (CC BY) license (https://creativecommons.org/licenses/by/4.0/).

1. Introduction

Oil sludges (multicomponent mixtures of oil products, soil, etc.) and petcoke are considered as toxic wastes hazardous for environment and human health [1–3]. Therefore, much effort is undertaken worldwide for the harmless treatment of oil sludges and petcoke, preferably with resource and energy recovery [4]. Currently, the most promising treatment technology is thermal processing of oil wastes with supercritical water [5],

steam [6], and carbon dioxide [7], especially when the heat required for waste processing is obtained using plasma [8,9], microwave discharges [10,11], or solar energy [12] rather than partial incineration of the feedstock. The advantages of steam and carbon dioxide as gasification agents (GAs) are well known [13]: (1) the off-gas does not contain diluent gases, (2) the required amount of GA is minimal due to the high specific heats of H_2O and CO_2, (3) the use of an H_2O/CO_2 blend allows controlling the off-gas composition, (4) the off-gas does not contain furans and dioxins [14], and (5) the amount of hydrogen produced by steam gasification of oil sludge is several times larger than that obtained by air-assisted gasification.

All gasification technologies can be divided, on the one hand, into autothermal and allothermal technologies and, on the other hand, to low-temperature and high-temperature technologies [15–18]. Autothermal technologies rely on the heat released in a gasifier due to partial oxidation of the feedstock in the added oxygen or air. Allothermal technologies use heat from external sources. Low-temperature gasification technologies include technologies with process temperatures below 1300 K [19]. The off-gas is usually contaminated with tars, CO_2, and particulates, as well as complex compounds of chlorine, sulfur, and heavy and alkali metals. Therefore, gas cleaning from various impurities is a necessary stage of such technologies. By-products of low-temperature gasification are solid residues called char and slag. Char is primarily composed of carbon, and may contain some oxygen, hydrogen, and inorganic ash. Slag is a safe glassy substance that can be used in the construction sector. The main drawbacks of low-temperature gasification technologies are the low yield and quality of the off-gas [20–22] and the complexity of controlling the technological process due to its long duration [22–24]. Current trends in the development of such technologies are mainly associated with the pre-treatment of oil sludges and petcoke and increasing their reactivity through the use of catalysts [25] and mixing with other types of feedstocks [26,27].

High-temperature gasification technologies include technologies with process temperatures above 1500 K [19]. Such temperatures are achieved during combustion and in plasma. The gasification products at such high temperatures are slag and high-quality off-gas. The off-gas mainly consists of CO and H_2 (syngas), and the content of hydrocarbons above C_2 is negligible. In this case, chlorine and sulfur compounds as well as compounds of heavy and alkali metals take on the simplest chemical structure. The main benefits of such gasification technologies are the high-quality off-gas due to the low content or complete absence of CO_2 and tars [28,29], high gasification efficiency due to the insignificant residues of tars and char [28,30], simple control of the off-gas quality due to the short residence time of feedstock in the gasifier and high off-gas yields due to the use of external energy sources to produce the heat required for gasification [31,32]. Nevertheless, plasma gasification technologies have some limitations. Thus, industrial-scale technologies based on arc and microwave plasma require enormous electrical power for the gas–plasma transition [33–37]. The latter looks irrelevant as the typical process temperature of plasma gasifiers is about 1600–2000 K, i.e., significantly lower than the temperature of the gas–plasma transition. In addition, there are limitations in the service life of expensive arc electrodes. The walls of plasma gasifiers must be manufactured using special structural materials with a refractory lining due to the high process temperatures. As for the efficiency of the microwave plasma gasification, it depends on feedstock properties [38].

The new high-temperature gasification technology patented by us in ref. [39] is free of the major drawbacks of plasma gasification technologies. This technology applies the pulsed generation of the H_2O/CO_2 mixture at a temperature exceeding 1800–2300 K and its pulsed supply to a gasifier as a GA at a very high velocity (about 1000 m/s). The capabilities of such a GA to gasify organic wastes without a negative environmental impact is well known [19]. The organic wastes are completely converted into the off-gas consisting only

of H_2 and CO in a proportion depending on the feedstock, whereas the mineral residue consists of aqueous solutions of oxygen-free acids, such as HCl, H_2S, HF, etc., and ammonia, as well as safe simple oxides [40,41]. The acids can be separated and concentrated and mineral residue can be used as additives in building materials. As for the gasifier, it can be fabricated from conventional structural materials and cooled by water because the gasification process mainly proceeds far from the walls, like in reciprocating engines.

The objectives of this study are to apply the new technology to the gasification of oil sludges and petcoke, and to find out whether this technology allows the complete processing of such feedstocks into useful products without using special structural materials and without emissions into the atmosphere and water bodies. Keeping in mind that this technology has been already implemented for other organic wastes like wood sawdust, sunflower seed husks, and waste machine oil [42], the novel and distinctive feature of the present study relies on the new type of feedstock employed.

2. Materials and Methods

2.1. Oil Wastes

In this work, three types of oil waste, namely, ground oil sludge (GOS), tank oil sludge (TOS), and petcoke are used. GOS is a heterogeneous viscous black liquid with a faint odor of hydrocarbons, with inclusions of clots, earth, and water (Figure 1a). The density of GOS is 1–1.15 g/cm^3. TOS is a black liquid, less viscous and more homogeneous than GOS, with a strong odor of light hydrocarbons (similar to paint) (Figure 1b). Its density is 0.9–0.95 g/cm^3. The petcoke is a product of secondary oil refining. It is a dark gray powder mainly with particles 100–1000 µm in size, but with inclusions of large aggregates up to 10–15 mm in size (Figure 1c). The bulk density of petcoke depends on the size of the fraction and is averaged at 1–1.1 g/cm^3.



(*a*) (*b*) (*c*)

Figure 1. Photographs of oil wastes: (**a**) GOS, (**b**) TOS, and (**c**) petcoke.

Samples of the oil wastes are studied by CHNS analysis on an automatic CHNS/O PE 2400 Series II analyzer (Perkin Elmer Inc., Shelton, CT, USA), and by IR and NMR spectroscopy on IRTracer-100 spectrometers (Shimadzu, Tokyo, Japan) and INOVA 400 MHz (Varian, Palo Alto, CA, USA). Accordingly, their higher heating value (HHV) is measured using the ABK-1V bomb calorimeter (Moscow, Russia). A brief description of the methods is given in Appendix A.

2.2. Gasification Technology

In this section, we provide a brief description of the new gasification technology. The oil waste supplied to the gasifier undergoes the pulse-periodic action of the GA generated in a pulsed detonation gun (PDG). Gasification products (off-gas) continuously flow out of the gasifier and are delivered to the customer either in full or in part. The latter occurs if part of the off-gas is used for PDG self-feeding. The PDG is a tube with one end equipped with ports for supplying fuel and oxidizer from manifolds with control valves and the other end attached to the gasifier. The operation cycle starts with the supply of combustible mixture components to the PDG: fuel (hydrogen or any hydrocarbon fuel) and oxidizer (oxygen, air, or air enriched with oxygen). After ignition of the combustible mixture with a spark plug, the arising flame accelerates and transitions to a detonation. The arising detonation wave further propagates in the mixture at a very high velocity (1800–2200 m/s), converting the mixture into the detonation products, mainly comprising steam and carbon dioxide at a temperature over 3300 K and pressure over 2.5 MPa. When the detonation wave arrives at the open end of the tube, the high-temperature detonation products expand to the gasifier in the form of a dense high-speed jet with a velocity over 1000 m/s (on average) leading to a rapid pressure drop in the PDG. Once the pressure in the PDG drops down to the pressure in the flow-through gasifier, new portions of fuel and oxidizer are supplied to the PDG. When the PDG is again filled with the combustible mixture, the next operation cycle begins by triggering the spark plug.

The PDG operates in a pulsed mode. The operation frequency is mainly determined by the time of the tube fill as this time is an order of magnitude longer than the total time required for flame ignition, acceleration, deflagration-to-detonation transition, and detonation wave propagation along the PDG. The average parameters (velocity, temperature, etc.) of the GA jet entering the gasifier are determined by the combustible mixture composition. The flow-through gasifier has a compact geometric shape to avoid the formation of long-lived stagnation zones promoting waste accumulation and slagging. The gasifier can be water cooled. Shock waves transmitted from the PDG to the gasifier exhibit enormous destructive power. On the one hand, they atomize the waste into fine particles and, on the other hand, they avoid particle agglomeration and adhesion to the gasifier walls. Under the action of successive incident and reflected shock waves, the waste particles, during their stay in the gasifier, undergo fragmentation due to both aerodynamic forces and impacts against the gasifier walls, whereas the particle fragments are repeatedly involved in high-temperature vortex structures of the GA away from the relatively cold walls. The gasifier includes devices for the continuous supply of waste and output manifolds for the continuous removal of gasification products (off-gas) and continuous/periodic removal of mineral residues. The time-averaged operation pressure in the gasifier is kept slightly higher than the atmospheric pressure to prevent the atmospheric air from being sucked in. Such gasification units can be currently designed using methods of computational fluid dynamics [43] and equilibrium gasification models [44–46]. The technology could be used for the gasification of both homogeneous and heterogeneous wastes. In particular, the latter could be composed of mixed solid (char) and liquid (tar) pyrolysis products of plastic solid waste [47].

2.3. Experimental Setup

The setup consists of the PDG, vertical gasifier, and off-gas cleaning system (Figure 2). The PDG is attached tangentially to the gasifier at its bottom. The off-gas flows out of the gasifier through the tube in its top cover. The PDG is a cylindrical tube with an internal diameter 50 mm and 900 mm long, i.e., the tube volume is 1.8 L. The PDG is equipped with a cooling jacket and a mixing-ignition device (MID). There are also two ports for installing

ionization probes (IPs) for measuring the detonation velocity. The distance between the ports is 250 mm. The combustible mixture used in the PDG is a near-stoichiometric methane-oxygen mixture with a fuel-to-oxygen equivalence ratio close to 1. The operation frequency of the PDG is 1 Hz. The average consumption of the methane-oxygen mixture is 3.75 ± 0.25 g/s. The gasifier is a standard gas cylinder with a volume of 40 L. The top flange of the gasifier is used to load the solid oil waste (petcoke) and remove the off-gas. The liquid oil waste (GOS and TOS) is fed into the gasifier continuously through the PDG just slightly upstream of the PDG exit to the gasifier. For this purpose, a special 2 L piston feeder is designed and manufactured. The solid oil waste (petcoke) is either loaded into the gasifier before the experiment in the form of a batch weighing 1 kg or mixed with TOS at a 1:1 mass ratio and fed into the gasifier in the form of a paste. In the latter case, the paste is fed to the gasifier in a similar way to the GOS and TOS. The gasifier walls have ports for installing a pressure sensor and thermocouples.

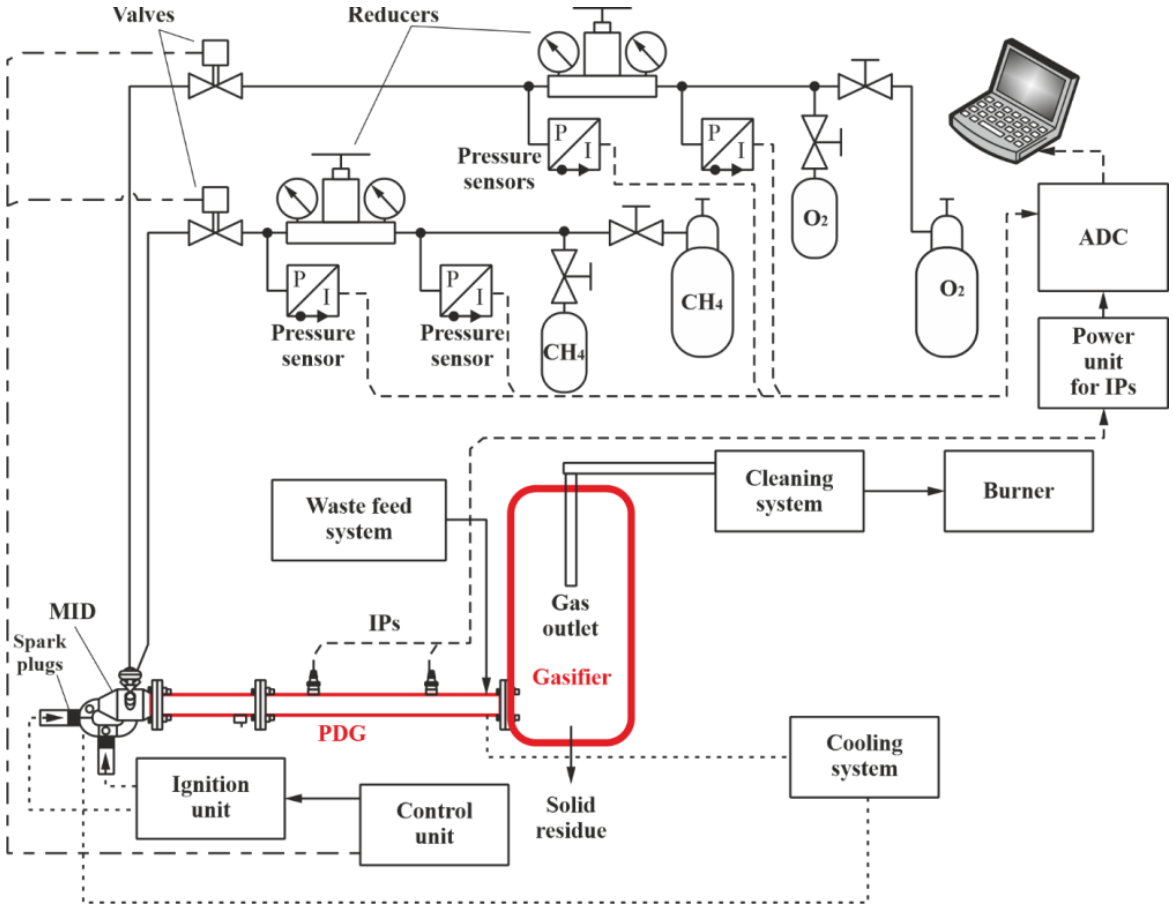

Figure 2. The experimental setup.

The off-gas flows out of the gasifier through a central channel with a diameter of 15 mm recessed into the gasifier by 300 mm relative to the upper flange and passing through the upper flange. The flow gas analyzer MRU VARIO Syngas (Fuchshalde, Germany), as well as the Chromatec-Crystal 2000 (Yoshkar-Ola, Russia) and GC-MS Chromatec-Crystal 5000 (Russia) gas chromatographs, are used for measuring the off-gas composition. The MRU VARIO gas analyzer records the volumetric concentrations of H_2, O_2, CO, CO_2, CH_4, and N_2. Since the MRU VARIO gas analyzer does not register hydrocarbons other than CH_4, these compounds (C_xH_y) are presented as N_2. The composition of C_xH_y is therefore studied by the other gas chromatographs. The concentration of H_2O in the off-gas is estimated by the mass of the condensate. The gas composition is displayed on the analyzer

screen and recorded in the memory unit. The error in measuring the concentrations is estimated at 5 vol.%.

The off-gas cleaning system consists of three cyclones, the off-gas cooling system, and the off-gas burner to burn the gasification products and to visually monitor the operation process. The off-gas first passes through the 5 L volume cyclone (large cyclone) and two 2 L cyclones (small cyclones). The first small cyclone is used to screen out solids. The second small cyclone mounted downstream the gas cooling system is used to collect condensate.

2.4. Experimental Procedure

The oil wastes are processed according to the following procedure. When using the liquid or paste wastes, the cyclic operation of the PDG starts without a waste supply and continues until the average temperature of the gasifier top reaches 870 K. Once this temperature is reached, the piston feeder begins to supply a feedstock to the PDG at a flow rate of 2–3 g/s. The average temperature of the upper part of the gasifier reaches 900 K. When using solid petcoke, a batch of waste weighing 1 kg is loaded into the gasifier before starting all systems. This option is evidently not optimal since the gasification process is accompanied by heating the entire waste batch and proceeds at a lower average temperature than with the continuous waste supply. Therefore, the temperature during the petcoke gasification increases from room temperature to 770 K with an average value of about 640 K.

It should be emphasized that the gasification reactions mostly proceed at the local instantaneous temperatures of the GA exceeding 2300 K. However, due to the spatial nonuniformity of the waste particle distribution in the gasifier and the nonuniform interaction of the waste particles with the GA jet, only part of the waste is exposed to such high temperatures. To improve the uniformity of GA–waste mixing, there is a need in efficient feeders for the solid-phase waste. The alternative suggested in this work is to produce a paste composed of sifted petcoke and TOS and to feed this paste by the piston feeder in the same way as the liquid oil sludges. This approach turned out much more effective than the one-time loading of a large batch of bulk petcoke into the gasifier.

2.5. Thermodynamic Model

The thermodynamic model of oil waste gasification is described in detail in ref. [44]. In the model, the PDG operates on the homogeneous mixture of fuel and oxidizer. Further, after ignition, the detonation wave forms and runs in the mixture, producing the detonation products consisting mainly of H_2O and CO_2 heated to a high temperature and compressed to a high pressure. After the detonation wave enters the gasifier, the detonation products expand to P_0 = 0.1 MPa and cool down. The oil waste fed into the gasifier is subjected to the thermochemical action of detonation products and is converted into the off-gas. The off-gas continuously flows out of the gasifier, cools down and is supplied to a customer.

The following assumptions are adopted in the model:

(1) The stoichiometric methane-oxygen mixture at normal conditions (P_0 = 0.1 MPa, T_0 = 300 K) is used for firing the PDG.
(2) The gasification of the oil waste proceeds at GA parameters (composition, temperature, and pressure), which are constant in time and correspond to the Chapman–Jouguet (CJ) state of detonation products expanded to P_0 = 0.1 MPa.
(3) The oil waste is represented by n-hexadecane ($C_{16}H_{34}$)—a physical and chemical surrogate for heavy petroleum fuels and lubricating oils often used in the literature [48]. The oil waste enters the gasifier with a temperature of $T_0 = 300$ K.
(4) The mixing of the oil waste with the GA proceeds instantaneously in the gas phase.

(5) The gasification of the oil waste is a constant pressure process without heat and mass exchange with the external environment.
(6) All the chemical reactions proceed in the gas phase.

The calculations are performed with the open access SDToolbox software (version 2021) [49] and the Cantera software (version 3.1.0) [50]. The former is used for determining the parameters of the detonation products, whereas the latter is used for determining the composition and thermodynamic parameters of the off-gas. The calculation procedure is divided into three stages. In the first stage, the composition, pressure, and temperature of the detonation products (GA) are calculated using the SDToolbox software. An additional solution to the $S, P = const$ problem is then used to determine the equilibrium parameters of the detonation products expanded to pressure P_0. In the second stage, the Cantera software is used to calculate the composition and temperature of the waste/GA mixture. The mixture temperature is determined by the waste/GA mass ratio and component temperatures. In the third stage, the Cantera software is used to solve the $H, P = const$ problem for the conversion of the waste/GA mixture into the off-gas in an adiabatic flow reactor at a constant pressure of 0.1 MPa and obtain the off-gas equilibrium composition and temperature. The software packages used herein (SDToolbox and Cantera) were previously thoroughly validated against available experimental and computational data on detonation velocities in gaseous fuel–air and fuel–oxygen mixtures as well as on compositions of detonation products and the off-gas produced by gasification of various organic wastes [44,51].

3. Results

3.1. Composition of Oil Wastes

Table 1 shows the results of the elemental analysis of the samples of the studied oil wastes. The accuracy of determining the composition is better than 0.30% abs. Noteworthy is the high content of carbon (77–85 wt.%), hydrogen (4–12 wt.%), and sulfur (2.1–3.5 wt.%) in the oil wastes, as well as the absence of ash in the TOS. The nitrogen content does not exceed 1%.

Table 1. Elemental analyses of oil wastes.

Oil Waste	C [a] %	H [a] %	N [b] %	S [c] %	Ash [a] %	Σel. %
GOS	76.63	11.15	up to 0.5 [e]	3.28	8.43	99.9
TOS [d]	84.96	11.98	0.56	2.14	–	99.64
Petcoke	82.38	3.88	1.00	3.53	7.00	97.79

[a] Express gravimetry method; [b] Dumas–Pregl–Korshun method; [c] Visual titration; [d] Analyses are carried out after drying with anhydrous sodium sulfate and filtration on a Schott filter POR111; [e] In the IR spectrum, signals of nitrogen-containing functional groups are not detected; Nitrogen atoms in the sample are contained in trace amounts or are virtually absent.

Figure 3 shows the IR spectra of the GOS (Figure 3a) and TOS (Figure 3b). The spectra of the studied samples are a set of absorption bands located in two spectral regions: from 2500 to 3000 cm^{-1} and from 680 to 1500 cm^{-1}, respectively. The absorption bands in the region from 2500 to 3000 cm^{-1} correspond to the asymmetric and symmetric stretching vibrations of the C–H bond in the $–CH_3$ and $–CH_2–$ functional groups. The absorption bands in the regions of 1377 cm^{-1} and 1462 and 1472 cm^{-1} correspond to the bending vibrations of C–H bonds of the $–CH_3$ and $–CH_2–$ functional groups, respectively. In the region of 740–890 cm^{-1}, bands are observed that reflect the vibration of C–C bonds in substituted aromatic compounds. The bands at 720 and 729 cm^{-1} correspond to the

pendulum vibrations of CH_2 groups. It is important to note that the samples do not contain water: there are no signals in the range from 3000 to 3500 cm^{-1}.

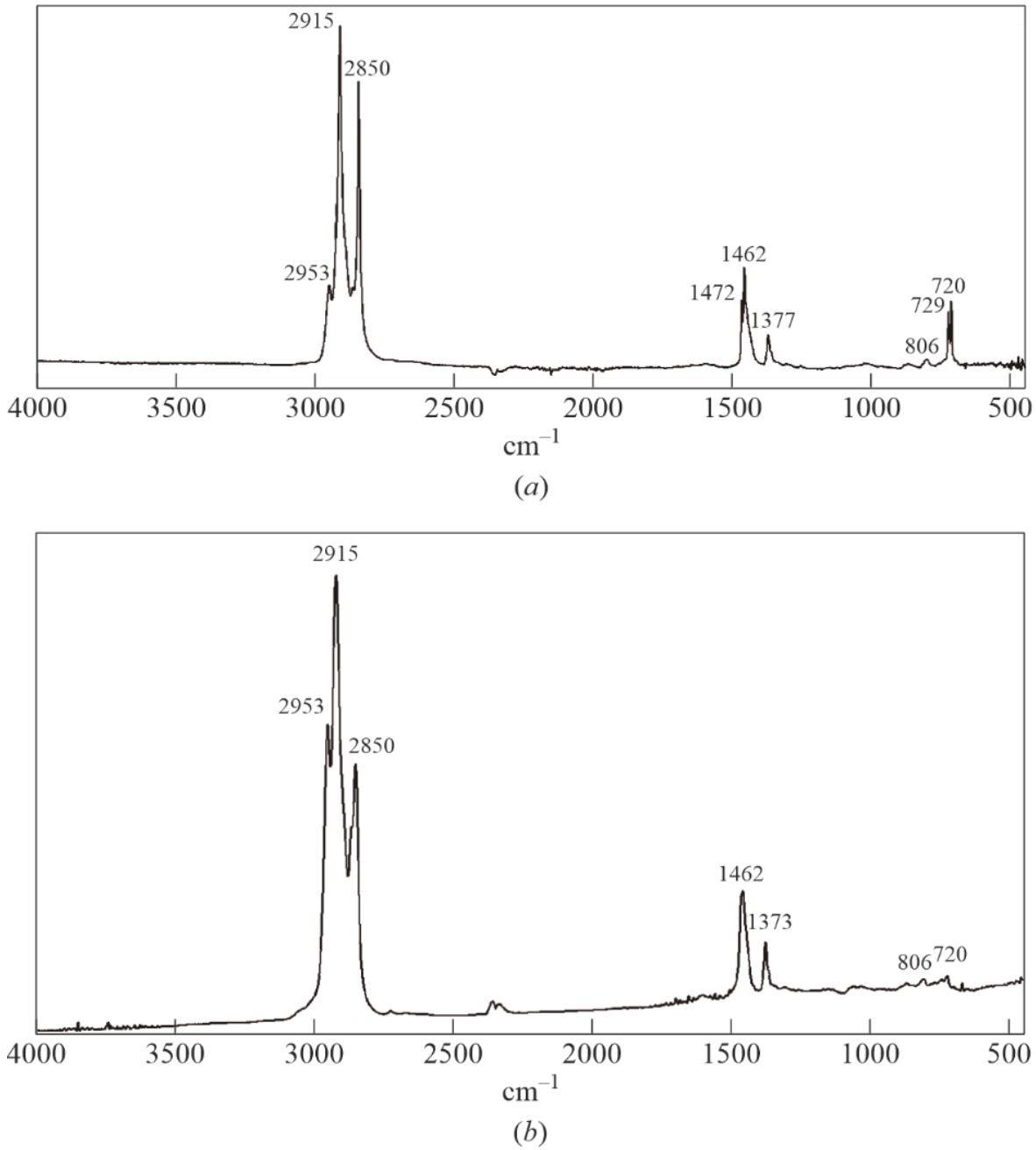

Figure 3. IR spectra of GOS (**a**) and TOS (**b**).

Figures 4 and 5 show the ^1H and ^{13}C NMR spectra of the GOS (Figure 4) and TOS (Figure 5) samples. The samples are dissolved in carbon tetrachloride CCl_4 and filtered from the mechanical particles. The spectra are recorded in CCl_4. It can be seen that the spectra for both wastes are almost identical. In the ^1H spectra in the range of 0.5–3.5 ppm, signals belonging to aliphatic hydrogen atoms are observed; and signals from aromatic hydrogen atoms are visible in the range of 6.5–8 ppm. The ^{13}C NMR spectra contain many different signals, with signals visible for carbon in CH_3 groups at 14.3 ppm and for CH_3 in aromatic groups at 20.0 ppm. Groups of signals that correspond to methylene CH_2 (22.8–35.0 ppm) and CH functional groups (36.3–40.0 ppm) are also visible. Aromatic

carbon signals are in the range of 125–130 ppm. The NMR spectra confirm the content of a small proportion of aromatic hydrocarbons in the oil sludge samples.

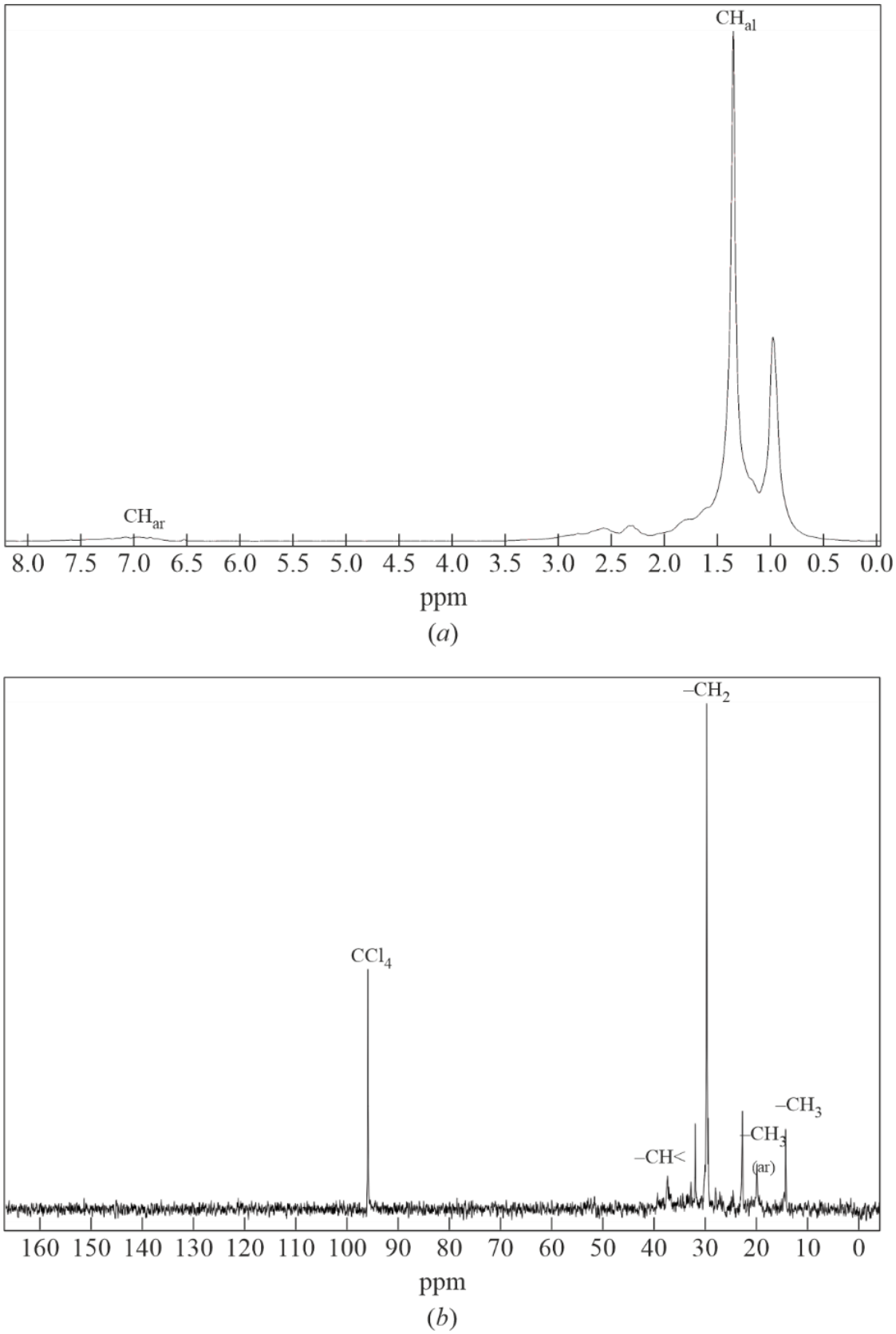

Figure 4. ^{1}H (**a**) and ^{13}C (**b**) NMR spectra of GOS.

Table 2 shows the data on the HHV, Q_S, of the tested oil sludges. The HHV of the TOS is 24% higher than that of the GOS, the Q_S value of the petcoke is 12% higher than that of the TOS.

Table 2. Higher heating values of original oil wastes.

Oil Waste	Q_S [a], MJ/kg
GOS	27.6 ± 0.117
TOS	36.4 ± 0.011
Petcoke	40.8 ± 0.414

[a] Bomb calorimetry method.

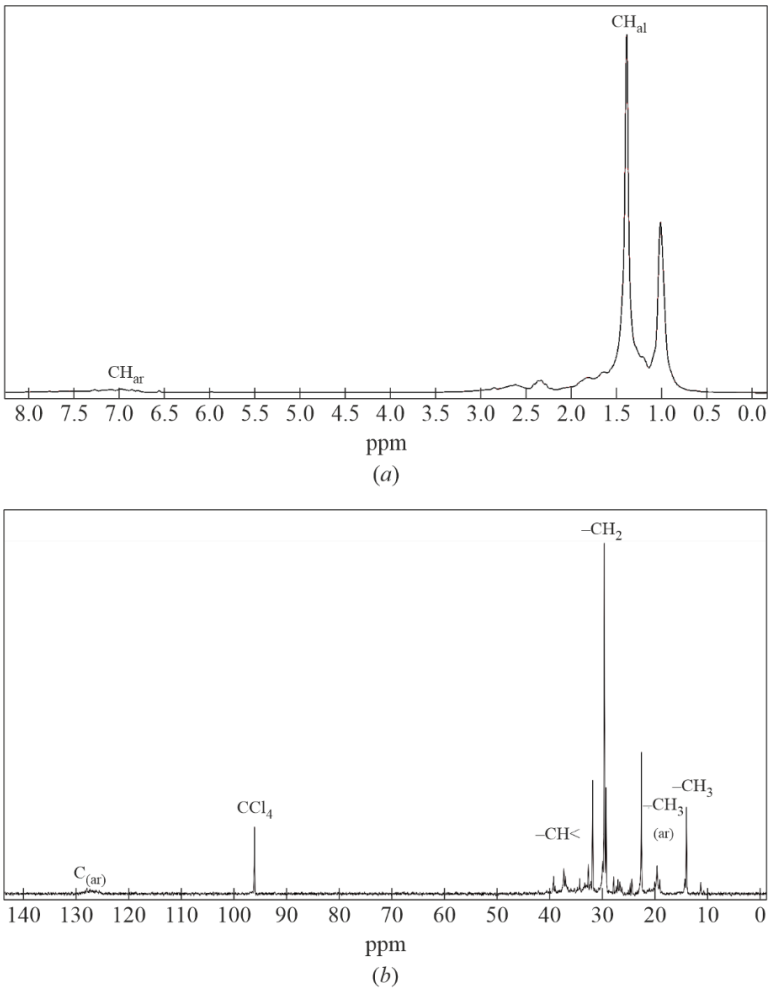

Figure 5. ^{1}H (**a**) and ^{13}C (**b**) NMR spectra of TOS.

Thus, according to the measurement data, the tested liquid oil sludges are the mixtures of branched aliphatic hydrocarbons with a small content of aromatic hydrocarbons and a large amount of carbon (77–85 wt.%) and sulfur (2.1–3.5 wt.%), and they possess an HHV of 28–36 MJ/kg. The solid petcoke possesses the largest HHV of about 41 MJ/kg.

3.2. Calculated Parameters of the Gasification Agent

A thermodynamic calculation is made to estimate the parameters of the GA obtained by the detonation of the stoichiometric methane-oxygen mixture. The calculated CJ detonation velocity is 2380 m/s (Mach number $M_{CJ} = 6.74$). The pressure, temperature, and density of the detonation products in the CJ state are 2.94 MPa, 3700 K, and 2 kg/m^3,

respectively. The temperature of the detonation products expanded to $P_0 = 0.1$ MPa is 2852 K. Table 3 shows the calculated equilibrium composition of the detonation products expanded to $P_0 = 0.1$ MPa.

Table 3. Calculated equilibrium composition of the GA at $P_0 = 0.1$ MPa.

Component	H_2O	CO_2	CO	H_2	O_2	O, H, OH
Content, vol.%	48	17	12	6	7	10

3.3. Setup Operation

Figure 6 shows an example of the records of two IPs in 13 consecutive operation cycles of the setup (Figure 6a) and an exploded view of one of the cycles (Figure 6b). The detonation wave propagates steadily from cycle to cycle at a velocity of 2100 ± 100 m/s. This velocity is somewhat lower than the thermodynamic value (2380 m/s), which may be caused by the incomplete mixing of the fuel components in the MID.

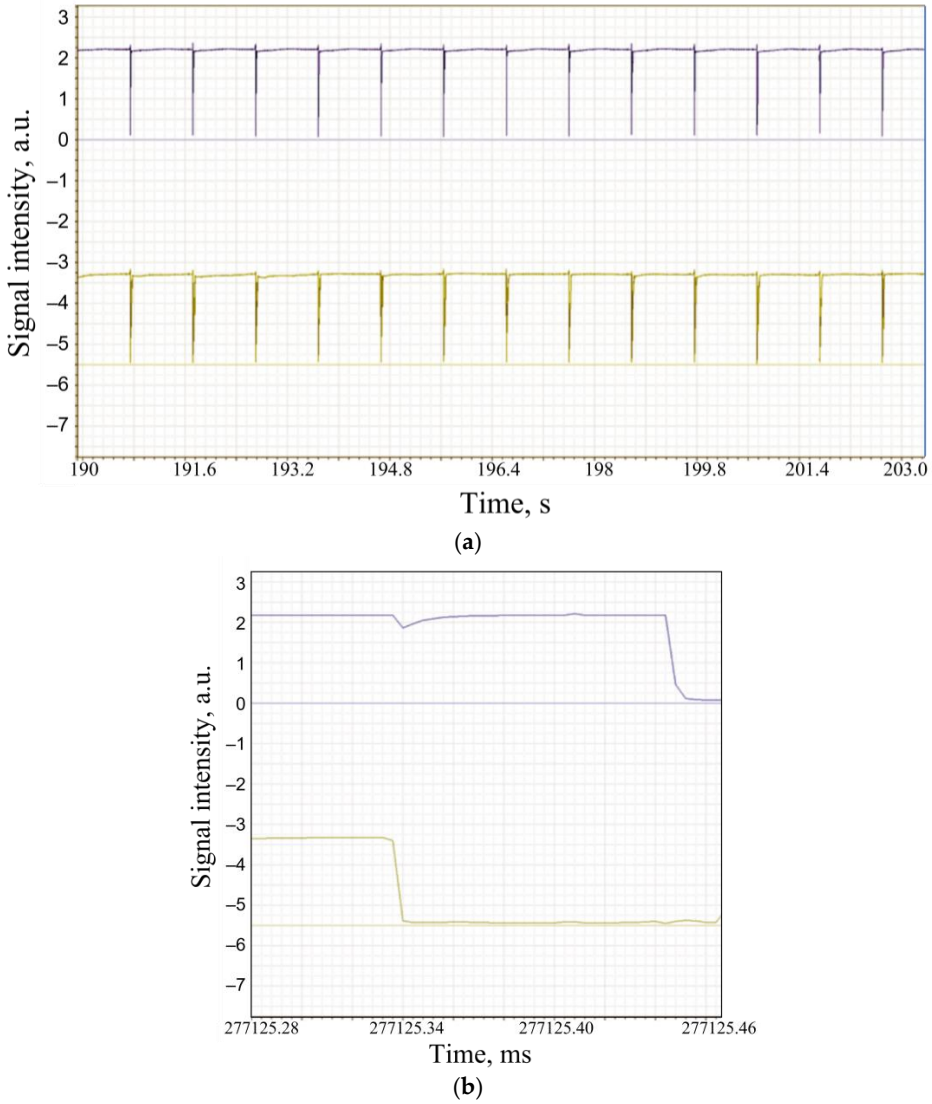

Figure 6. Examples of IP records during PDG operation in the frequency mode: (**a**) records in 13 consecutive cycles, (**b**) enlarged view of the record in a single cycle.

Figure 7 shows examples of the records of the gasifier wall temperature, T_w, and gas temperature, T_g, in the upper part of the gasifier. After reaching the operation mode

that could be treated as the quasi-steady-state gasification, the wall and gas temperatures are seen to be approximately equal (the junctions of the thermocouple measuring gas temperature are located near the gasifier wall).

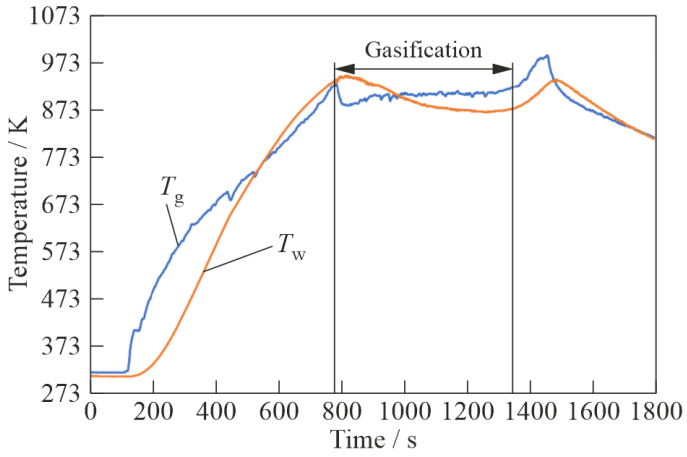

Figure 7. Examples of records of the gasifier wall temperature T_w and gas temperature T_g in the upper part of the gasifier.

3.4. Off-Gas Composition

Figure 8 shows an example of gas analyzer records in the experiment with the gasification of TOS. In this experiment, a total mass of liquid TOS equal to 1300 g is loaded into the feeder. The overall duration of the gasification process is seen to be about 800 s at an average waste flow rate of 2.5 mL/s. The quasi-steady-state gasification process lasts approximately $\Delta \approx 660$ s. At the completion of the gasification process, the off-gas contains 33 vol.% H_2, 40.4 vol.% CO, 15.6 vol.% CO_2, 7.2 vol.% CH_4, 0 vol.% O_2, and 3.8 vol.% C_xH_y, i.e., the off-gas consists of 84.4% flammable gas. The average temperature of the gasifier wall in this experiment reaches 850 K, and the average overpressure in the gasifier is 0.035 MPa. The bottom flange of the gasifier is used to extract the solid mineral residue. After the experiment, the mass of an extracted ash residue is about 100 g.

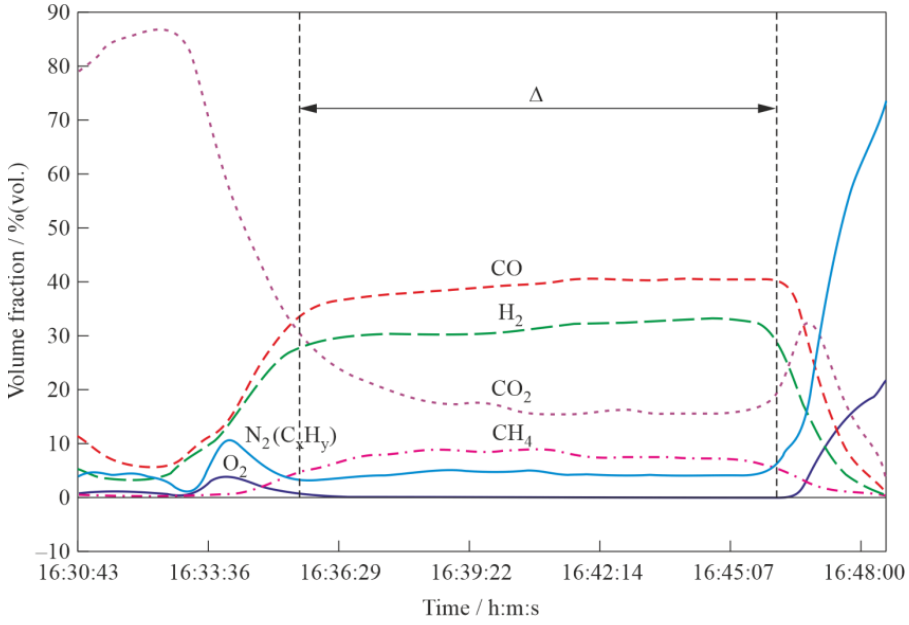

Figure 8. Records of gas analyzer in an experiment with liquid TOS; Δ is the duration of the quasi-steady-state gasification process.

Figure 9 shows an example of gas analyzer records for the case when a 1 kg batch of solid petcoke is loaded into the gasifier before the experiment. The overall operation time is about 1080 s and the time of the quasi-steady-state gasification process is $\Delta \approx 720$ s. At the completion of the gasification process, the off-gas contains 29 vol.% H_2, 42.1 vol.% CO, 19.2 vol.% CO_2, 5.6 vol.% CH_4, 2 vol.% O_2, and 2.0 vol.% C_xH_y, i.e., the off-gas consists of 78.8% flammable gas. During the experiment, the temperature of the gasifier wall increases from the room temperature to 770 K so that the average temperature is about 640 K. After the experiment, the mass of the ash residue extracted from the cyclones as a very fine powder is about 400 g.

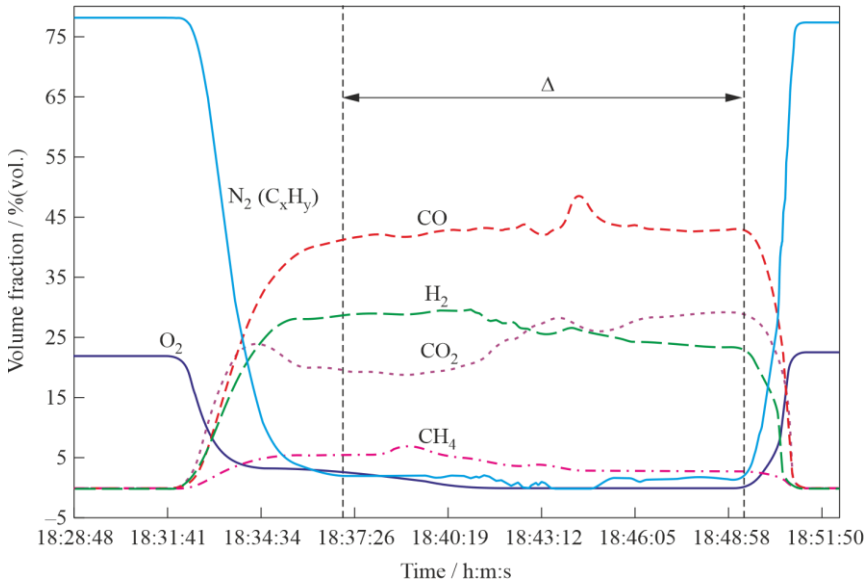

Figure 9. Records of gas analyzer in an experiment with solid petcoke; Δ is the duration of the quasi-steady-state gasification process.

Figure 10 shows an example of the gas analyzer records for the case when a mixture of TOS and petcoke in the form of a paste is continuously fed into the gasifier. The overall operation time is about 1200 s with the duration of the quasi-steady-state gasification process $\Delta \approx 720$ s. At the completion of the gasification process, the off-gas contains 29 vol.% H_2, 40 vol.% CO, 20.8 vol.% CO_2, 6.2 vol.% CH_4, 0 vol.% O_2, and 4.1 vol.% C_xH_y, i.e., the off-gas consists of 79.2% flammable gas. The temperature of the gasifier wall reaches 870 K. The average overpressure in the reactor is 0.04 MPa. Feeding the paste turns out to be much more efficient than directly loading petcoke into the gasifier.

Table 4 shows the cumulated results of the experiments. The following notations are used: M_0 is the initial mass of oil waste, m is the mass of ash residue, q_S is the waste mass flow rate, t is the gasification time, T_w is the gasifier wall temperature, and Q'_g and Q_g are the calculated volumetric and mass-related HHV of the off-gas, respectively. The table additionally shows the measured volume fractions of the off-gas components.

The mass flow rates of the waste, q_S, and GA, $q_{GA} = q_f + q_{ox}$ (q_f and q_{ox} are the mass flow rates of the fuel (methane) and oxidizer (oxygen)), in the experiments are 2–3 and 3.5–4 g/s, respectively, i.e., the waste/GA mass ratio varies from 0.5 to 0.85. The dry off-gas contains 80–90 vol.% flammable gas (the only nonflammable component is CO_2). The typical composition is 28–33 vol.% H_2, 40–45 vol.% CO, 10–20 vol.% CO_2, 5–10 vol.% CH_4, 0–3% O_2, and 4–7% C_xH_y. The GC-MS chromatograms indicate that C_xH_y in the off-gas is represented by C_2–C_3 noncondensable hydrocarbons like C_2H_4, C_2H_6, and C_3H_8, i.e., the off-gas is free of tar. The typical measured gasifier wall temperature is $T_w = 850$–900 K. The HHV of the dry off-gas is 12–18 MJ/kg.

Table 4. Summary table for performed experiments.

Oil Waste	M_0, g	m, * g	m/M_0	q_S, g/s	t, s	T_w, K	CO_2, %	CO, %	H_2, %	CH_4, %	C_xH_y, %	O_2, %	Q_g' **, MJ/m^3	Q_g, MJ/kg
GOS	1680	150	0.09	3.1	550	900	19.6	36.2	28.8	9.0	6.0	0	15.1	14.7
GOS	1840	30	0.08	3.7	500	800	13.5	39.8	31.3	9.0	6.3	0	16.0	16.7
TOS	1520	0	–	2.2	690	900	13.1	40.6	32.1	8.5	5.4	0,2	15.4	16.3
TOS	1520	–	–	2.6	580	890	11.8	39.7	31.1	11.0	6.5	0	16.8	17.9
TOS	1300	100	0.07	2.3	660	850	15.6	40.4	33.0	7.2	3.8	0	13.9	14.5
petcoke	1000	700	0.70	–	420	620	16.2	42.8	28.3	5.7	4.0	3	13.3	13.5
petcoke	1000	400	0.40	–	720	640	19.2	42.1	29.0	5.6	2.0	2	11.8	11.8
TOS–petcoke paste (1:1)	3520	490	0.14	2.4	720	870	20.8	40.0	29.0	6.2	4.1	0	13.3	12.7

* Ash residue extracted from cyclones; ** HHV and density for C_xH_y are taken to be equal to 70 MJ/m^3 and 1.6 kg/m^3, respectively.

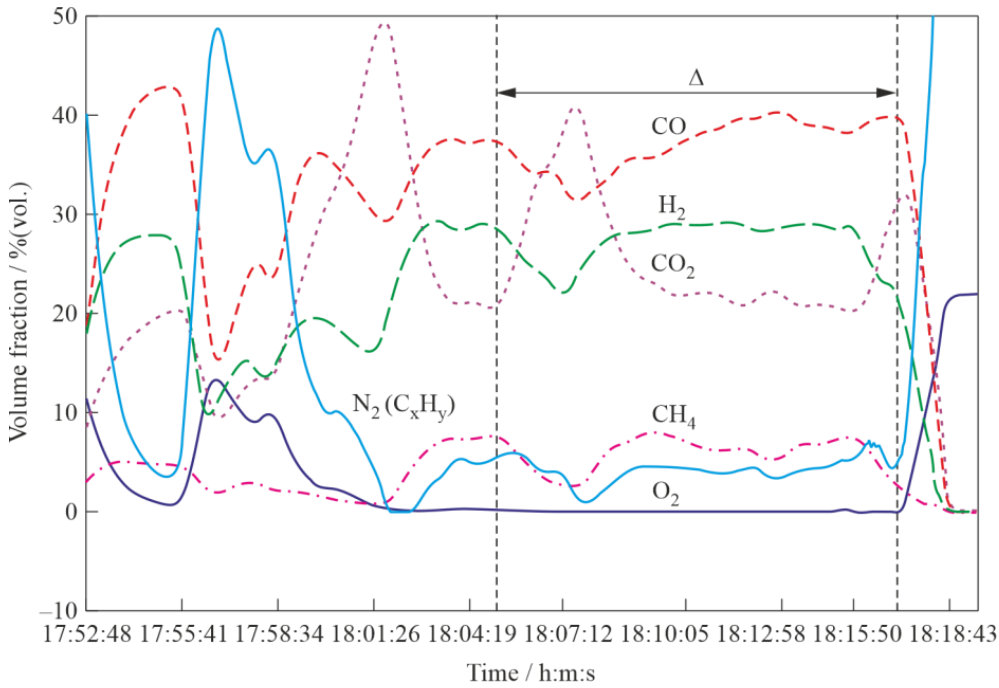

Figure 10. Records of a gas analyzer in an experiment with the supply of a TOS–petcoke paste (1:1); Δ is the duration of the quasi-steady-state gasification process.

3.5. Ash Residues

At the completion of the gasification process, ash residues in the gasifier are absent: all the ash residues are taken from the cyclones. This means that the gasification process is accompanied by mass loss from the gasifier in the form of fine solid particles, and the degree of carbon conversion in such particles can vary within wide limits. The maximum amount of ash residues extracted from the cyclones is observed during the gasification of the petcoke (up to 70%!). When using the TOS–petcoke paste (1:1), the mass loss from the gasifier is reduced to 14–15%. The gasification of the GOS and TOS is accompanied by a smaller mass loss of 7–10%.

Figure 11 shows a photograph of the ash residue extracted from the large and small cyclones during the oil waste gasification, as well as the volume share per size interval of the ash particles for all four types of oil waste under study, namely, the GOS, TOS, petcoke, and TOS–petcoke paste (1:1). The particle size distributions are measured by wet laser diffraction using the Analysette22 (Fritsch) device in the presence of a surfactant during ultrasonic treatment (50 W) (see Appendix B). The analysis of the particle samples

taken from the large cyclone for each type of oil waste shows that all the samples possess particle sizes around 1 μm (0.7–1.2 μm). The particles extracted from the small cyclones are hundreds of nanometers in size. The composition and mass of the ash residue are used to assess the carbon conversion during the gasification process.

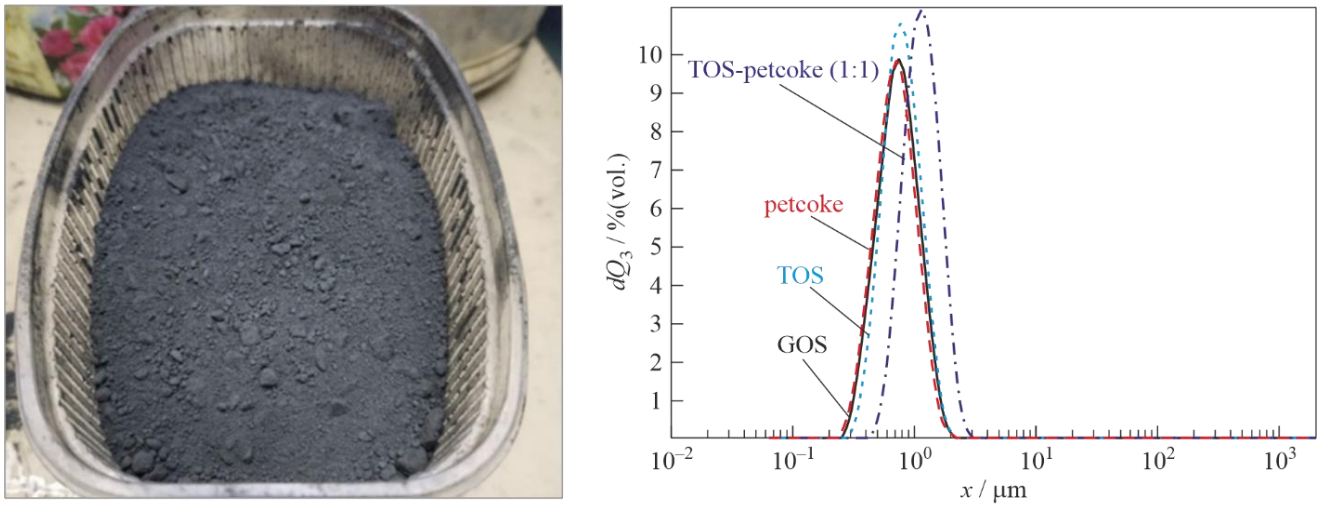

Figure 11. (**a**) Photograph of ash residue extracted from the large and small cyclones of the off-gas cleaning system after experiment, and (**b**) size distributions of ash particles averaged over three samples for four types of oil waste: 1—GOS, 2—TOS, 3—petcoke, and 4—TOS–petcoke paste (1:1).

Table 5 shows the elemental composition of the fine ash residues from the studied oil wastes. As one could expect, significant mass loss from the gasifier during the gasification of the petcoke leads to a low carbon conversion: the residual carbon content reaches 90–91% in the ash particles of the petcoke and TOS–petcoke paste (1:1), 81% in the ash particles of the TOS, and 27% in the ash particles of the GOS. The hydrogen content in the ash residues decreases several times (down to 1–2 wt.%). The nitrogen content in the ash residues of all the studied oil wastes turns out to be almost the same as in the feedstock (at a level of 1 wt.%). The sulfur content in the ash residues of the GOS decreases by a factor of five compared to the original feedstock, while its content in the TOS and petcoke remains approximately the same as in the original feedstock. Considering a sulfur content of 2.1–3.5 wt.% on the GOS, TOS, and TOS–petcoke paste feeding and yields of corresponding ash residues of at most 7–14 wt.% (as shown in Table 4), it is clear that a normalized final 0.2–0.4 wt.% S (only 5–10% of the starting sulfur) is retained in the ash residues. The remaining 90–95% is obviously converted to the gas-phase compounds. Due to the high concentrations of hydrogen in the gasification products of the oil wastes (28–33 vol.%) and a lack of free oxygen in the GA, it can be assumed that the sulfur present in the feedstock reacts with hydrogen, forming flammable hydrogen sulfide H_2S, which, together with the aqueous condensate, produces a weak aqueous solution of hydrogen sulfide acid. Importantly, all three devices used for measuring the composition of the off-gas (Chromatec-Crystal 2000 and GC-MS Chromatec-Crystal 5000 gas chromatographs and MRU VARIO flow gas analyzer) showed very similar results despite different operation principles. This indicates that such compounds as H_2S are not present in the dry off-gas. It should also be noted that the smell of hydrogen sulfide was not present during the experiments. The issue of the formation of gaseous sulfur compounds during the gasification of oil waste will be studied further.

Table 5. Elemental composition of oil-waste ash residues.

Oil Waste	Mass, mg	H, %	C, %	N, %	S, %	Ash, %	Σel., %
GOS	5.082	1.00	26.98			69.93	
	10.168			0.91			99.4
	16.474				0.58		
TOS	3.956	1.63	81.33			15.82	
	9.356			1.20			102.97
	13.376				2.99		
Petcoke	5.358	1.20	91.52			-	
	10.514			1.03			96.63
	11.740				2.88		
TOS–Petcoke paste (1:1)	3.498	0.97	90.83			7.02	
	10.344			0.88			101.93
	13.302				2.23		

Table 6 shows the values of HHV, Q_{Sa}, for the fine ash residues of the studied oil wastes, which generally confirm the results of the elemental analysis. Significant mass loss from the gasifier during the gasification of the petcoke and liquid paste leads to high values of HHV for the ash residues. The carbon content in the ash residues can be roughly estimated by the ratio Q_{Sa}/Q_S. The results definitely indicate that special measures are needed to reduce the mass loss from the flow gasifier.

Table 6. The values of HHV for oil-waste ash residues.

Oil Waste	Q_{Sa}, MJ/kg	Q_{Sa}/Q_S
GOS	9.14 ± 0.090	0.33
TOS	32.8 ± 0.3	0.90
Petcoke	29.7 ± 0.3	0.73
TOS–Petcoke paste (1:1)	32.9 ± 0.3	0.85

The specific surface area and porous structure of the ash particles are studied by low-temperature sorption of nitrogen at 77 K. The measurements are performed using the NOVA 1200e gas sorption analyzer (Quantachrome Instruments, Boynton Beach, FL, USA). Highly purified nitrogen gas is used as an adsorbate. Before measurements, the samples are degassed in vacuum at 473 K for 3 h.

Figure 12 shows the nitrogen adsorption and desorption isotherms for the ash residue particles of all the studied oil wastes at the plane "specific volume V—relative pressure P/P_s" (P_s is the saturated vapor pressure of the adsorbate at the experimental temperature). Despite the samples showing a low sorption capacity, the isotherms of each sample exhibit hysteresis between the adsorption and desorption branches, which indicates their mesoporous structure. For the petcoke, the hysteresis does not close down at low relative pressures P/P_s. This type of hysteresis is often observed for polymer structures and is explained by the "swelling" of the polymer during adsorption. It is possible that for the petcoke, this is explained by similar processes.

Table 7 shows the measured values of the specific surface area S_{BET} and the parameters of the porous structure of the ash residue particles of all four studied oil wastes. The specific surface area S_{BET} is determined using the Brunauer–Emmett–Teller (BET) method [52] in the range of relative pressure P/P_s = 0.05–0.21. The pore size distribution is determined using the Barrett–Joyner–Halenda (BJH) method [53] for the desorption branch of the isotherm, assuming a cylindrical pore geometry.

Figure 13 shows the pore size distributions in the ash residue particles for all four studied oil wastes. The TOS and petcoke ash residues show a sharp peak for pores with a diameter of 3.9 nm and a wide falling trail down to 40–50 nm, i.e., mesopores with a wide range of sizes. The ash residue of the TOS–petcoke paste (1:1) can be characterized by

a wide range of mesopores of 3 to 50 nm in size with a weak peak at 3.9 nm. The GOS ash residue shows the minimum pore volume and, accordingly, the smallest specific surface area. In principle, it could be classified as a nonporous ash; however, it shows a slight hysteresis and formally can also be classified as a mesoporous ash.

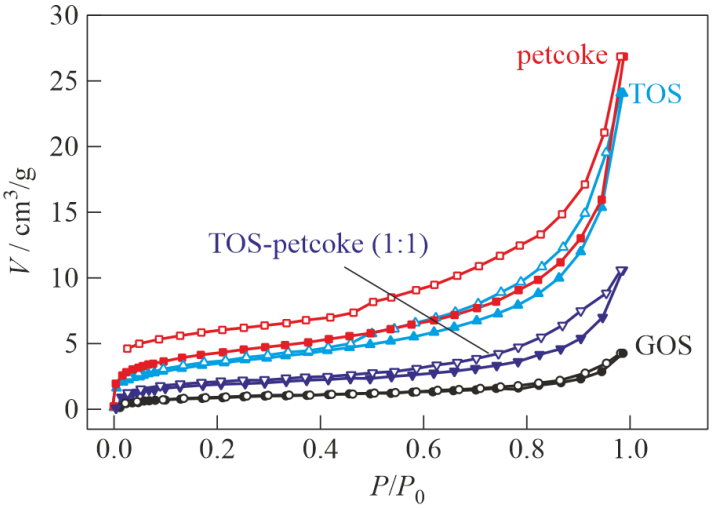

Figure 12. Adsorption (filled symbols) and desorption (empty symbols) isotherms of nitrogen at 77 K for the studied samples of ash residue particles: 1—GOS, 2—TOS, 3—petcoke, 4—TOS–petcoke paste (1:1).

Table 7. Specific surface area and parameters of the porous structure for ash residue particles of oil wastes.

Waste	S_{BET} [a] m²/g	V_t [b] cm³/g	d [c] nm	V [c] cm³/g	S [c] m²/g
GOS	3.3	0.007	3–40	0.006	1.6
TOS	12.5	0.037	3.9 4–50	0.036	11.4
Petcoke	15.2	0.042	3.9 4–50	0.037	12.1
TOS–Petcoke paste (1:1)	6.9	0.016	3–40	0.015	4.6

[a] Specific surface area according to the BET method. [b] Total pore volume at $P/P_s = 0.99$. [c] Diameter, total volume, and area of pores according to the BJH method.

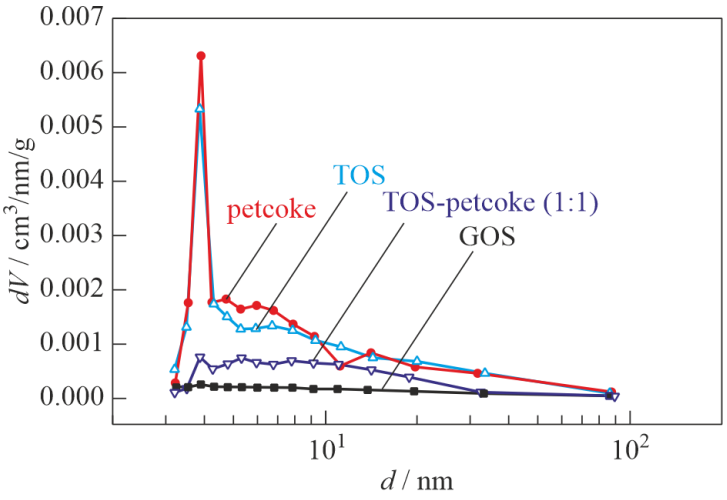

Figure 13. Pore size distributions in ash residue particles of all studied oil wastes measured by the BJH method: 1—GOS, 2—TOS, 3—petcoke, 4—TOS–petcoke paste (1:1).

4. Discussion

It is interesting to compare different gasification technologies in terms of the off-gas composition and process parameters like dry gas yield (DGY), carbon conversion efficiency (CCE), cold gas efficiency (CGE), and net power efficiency (NPE). The DGY is the ratio of the volumetric flow rate of the off-gas to the mass flow rate of the waste. The CCE is the ratio of the carbon in the off-gas to the carbon fed to the reactor with the waste and GA. The CGE is the ratio of the LHVs of the off-gas and waste and describes the potential process efficiency for further applications of the off-gas. The NPE is the ratio of the produced off-gas LHV to the sum of the waste LHV and the external energy needed for off-gas production [54]. In contrast to the CGE, the NPE includes the energy needed for obtaining a high-temperature GA in the energy balance. As an example, we compare the results of the TOS gasification at a waste/GA mass ratio of 0.5 with the results of the biomass gasification in a dual bubbling fluidized bed gasifier [55]. The DGY, CCE, CGE, and NPE are calculated as:

$$DGY = \frac{q_g}{q_S} 100\%$$

$$CCE = \left(X_{C0}^{-1} \sum_{i=CO,CO_2,CH_4,\ldots} X_i \right) 100\%$$

$$CGE = \frac{q_g Q'_{gL}}{q_S Q_{SL}} 100\%$$

$$NPE = \frac{q_g Q'_{gL}}{q_S Q_{SL} + q_f Q_{fL} + q_{ox} Q_{ox}} 100\%$$

where q_g is the volumetric flow rate of the dry off-gas (Nm^3/s); q_S, q_f, and q_{ox} are the mass flow rates of the waste, fuel (methane or LPG [55]), and oxidizer (oxygen), respectively (kg/s); X_{C0} is the number of carbon moles in the unit mass of the waste and GA; X_i is the number of carbon moles in the carbon-containing species in the product off-gas; Q'_{gL} is the off-gas LHV (MJ/Nm^3); Q_{SL} is the waste LHV (MJ/kg); Q_{fL} is the fuel (methane or LPG [55]) LHV (MJ/kg); and Q_{ox} is the energy needed for oxygen production (1.1 MJ/kg [56]). Note that for the conditions in ref. [55], $q_{ox} = 0$.

Table 8 compares the corresponding off-gas compositions, LHV, DGY, CCE, CGE, and NPE. Since the technology used herein utilizes oxygen rather than air, the off-gas contains no nitrogen and considerably more CO (40.4 vol.% vs. 23.2 vol.% in ref. [55]), while the contents of hydrogen in the off-gas are comparable (33 vol.% vs. 34.8 vol.%). Since the technology used herein exhibits a higher process temperature, the contents of CO_2 and CH_4 are lower (15.6 vol.% vs. 19.7 vol.% and 7.2 vol.% vs. 10.6 vol.%, respectively) and tar is completely absent (in contrast to 12.4 g/Nm^3 in ref. [55]). Owing to a smaller content of CO_2, the off-gas LHV is 15% higher than in ref. [55]: 12 vs. 10.5 MJ/kg. The main differences appear in the values of DGY, CCE, and CGE. The value of DGY is a factor of 2.4 larger than in ref. [55] due to the absence of tar and char in the gasification products. The values of CCE and CGE obtained herein are seen to be 95% and 107% as compared to 73% and 77% reported in ref. [55], respectively. Note that values of CGE exceeding 100% have been reported in the literature [54,57–60]. As for the NPE, it is comparable with that reported in ref. [55]: 70% vs. 66%. The NPE of the technology under consideration can be improved in several ways. Firstly, a part of the produced off-gas can be utilized in the PDG, thus completely replacing the fuel (methane). According to ref. [44], about 30% of the off-gas produced by the gasification of waste machine oil must be used for this purpose. In this case, the stoichiometric amount of oxygen fed to the PDG will be considerably decreased as the recirculating off-gas is mainly composed of H_2 and CO.

Secondly, the oxygen fed to the PDG can be replaced by oxygen-enriched air [44]. Thirdly, the process temperature could be increased by increasing the operation overpressure in the gasifier [44]. Fourthly, the energy produced from off-gas cooling can also be utilized in the process. These modifications to the technology will be a subject of future work.

Table 8. The compositions of the off-gas obtained by the thermomechanochemical gasification of oil sludges and by the biomass gasification in a dual bubbling fluidized bed gasifier [55].

Waste	H_2, vol.%	CO, vol.%	CO_2, vol.%	CH_4, vol.%	C_xH_y, vol.%	N_2, vol.%	Tar, g/Nm^3	HHV, MJ/kg	DGY, Nm^3/kg	CCE, %	CGE, %	NPE, %	Ref.
Biomass	34.8	23.2	19.7	10.6	-	7.3	12.4	10.5	1.33	73	77	66	[55]
TOS	33.0	40.4	15.6	7.2	3.8	0	0	12.0	3.2	95	107	70	This work

Figure 14 presents the calculation results for the equilibrium states of the off-gas of the oil waste gasification depending on the waste/GA mass ratio. The parameters of the GA in the calculations are obtained by expanding the detonation products of the stoichiometric methane-oxygen mixture to $P_0 = 0.1$ MPa. The thick dashed curve corresponds to the equilibrium temperature, and the thin curves correspond to the equilibrium volume fractions of the off-gas components. The wide bar labeled "Uniform distribution" approximates the experimental range of the waste/GA mass ratio in the present study.

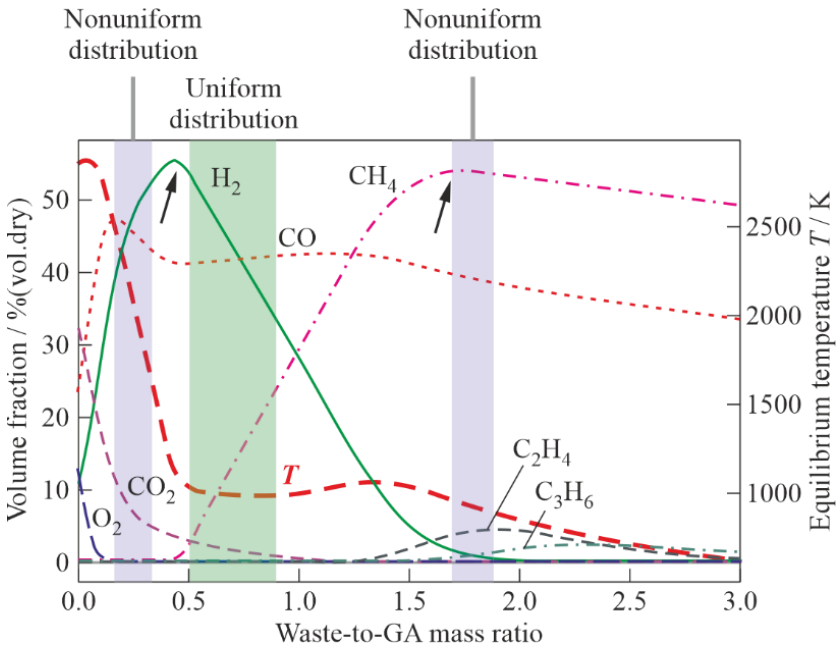

Figure 14. The equilibrium parameters of the dry off-gas of oil waste gasification vs. the waste/GA mass ratio. The GA is represented by the detonation products of the stoichiometric CH_4–O_2 mixture expanded to atmospheric pressure. Thin curves correspond to the volume fractions of gaseous components. The thick dashed curve corresponds to temperature. The wide vertical bar corresponds to the experimental range of the waste/GA mass ratio in the present study. Two narrow vertical bars conditionally show two possible local waste/GA mass ratios in the gasifier caused by the spatial nonuniformity of waste distribution.

The measured temperatures of the gasifier wall (T_r = 870–900 K, see Table 4) are in reasonable agreement with the calculated value of the thermodynamic equilibrium temperature of the gasification products (approximately 1000 K), if one takes into account that the gasifier wall is not thermally insulated.

The measured contents of CO (40–45 vol.% dry) and CH_4 (5–10 vol.% dry) in the off-gas are in reasonable agreement with the thermodynamic calculation (41 vol.% dry

and 3–23 vol.% dry, respectively). The measured lower contents of H_2 (28–33 vol.% dry instead of calculated 55.4 vol.% dry) and measured higher contents of CO_2 (10–20 vol.% dry instead of calculated 3.4 vol.% dry) and C_xH_y (4–7 vol.% dry instead of calculated 0 vol.% dry) could be associated with several reasons.

The first reason is the possible nonuniform distribution of the waste/GA mass ratio in the gasifier. As a matter of fact, during the aerodynamic breakup/spraying of the liquid/solid oil waste in the gasifier, there are zones with both low and high local waste/GA mass ratios. If one takes this fact into account, e.g., in the form of the two local waste/GA mass ratios shown in Figure 14 as narrow vertical bars labeled "Nonuniform distribution", then the average mass fraction of H_2 in the off-gas will obviously decrease, whereas the mass fractions of CH_4, CO_2, and C_xH_y will obviously increase compared to the ideal values when the waste is uniformly distributed in the GA (as presumed in the thermodynamic calculation). As for the mass fraction of CO, it weakly depends on the waste/GA mass ratio, with the exception of the region of small waste/GA mass ratios (less than 0.2), unlike other components. Thus, to increase the yield of H_2, it is necessary to improve the mixing of the waste with the GA. To check the importance of this factor, we installed a helical tube insert between the PDG and the gasifier (Figure 15). Preliminary tests with the TOS showed that this modification led to a decrease in the CO_2 and C_xH_y contents from 10–20 vol.% to 5 vol.% and from 4–7 vol.% to 2 vol.%, respectively, and to an increase in the H_2 content to 40 vol.%, i.e., it shifts the off-gas composition closer to the thermodynamically calculated composition.



Figure 15. The helical tube insert installed between the PDG and the gasifier for improving the mixing between waste and GA.

The second reason is the possible influence of temperature gradients in the gasifier on the off-gas composition. This effect was studied in ref. [43] by the three-dimensional CFD simulation of the operation process in the gasifier with two oppositely directed PDGs operating at a frequency of 5 Hz. It is shown in ref. [43] that the decrease in the gasifier wall temperature from 850 to 450 K decreases the time- and mass-averaged process temperature in the gasifier from 2250 to 2200 K, i.e., by only 50 K. This led the authors of ref. [43] to the conclusion that the gasifier could be manufactured using conventional structural materials and could be water cooled as the wall temperature does not play a significant role in the gasification process.

Interestingly, in accordance with the thermodynamic calculation, the composition with the maximum content of H_2 or the composition with the maximum content of CH_4 can be selected as the target composition of the produced dry off-gas. In Figure 14, these compositions are indicated by arrows. The off-gas of the first target composition is characterized by an H_2 content of 55.4 vol.% dry with 41 vol.% dry CO, 3.4 vol.% dry CO_2, 0.2 vol.% dry CH_4, a temperature of 1121 K, and a lower calorific value (LHV) of 19.9 MJ/kg. This off-gas can be referred to as the syngas as the H_2/CO ratio of such a gas is equal to 1.35, which is appropriate for the synthesis of methanol and synthetic motor fuels. This syngas is obtained by adding 0.45 kg waste to 1 kg GA. If, instead of the waste/GA mass ratio, one uses the waste/methane mass ratio, it appears that with the help of 1 kg methane and 4 kg oxygen it is possible to gasify 2.2 kg oil sludges and obtain 7.2 kg syngas of the specified composition. The off-gas of the second target composition is characterized by a CH_4 content of 53.9 vol.% dry with 39.3 vol.% dry CO, 1.2 vol.% dry H_2, 4 vol.% dry C_2H_4, 0.7 vol.% dry C_2H_2, 0.8 vol.% dry C_3H_6, a temperature of 952 K, and an LHV of 33.6 MJ/kg. This off-gas can be referred to as energy gas as it exhibits a high LHV and can be used for the production of heat and electricity. This energy gas is obtained by adding 1.73 kg waste to 1 kg GA. If, instead of the waste/GA mass ratio, one uses the waste/methane mass ratio, it appears that with the help of 1 kg methane and 4 kg oxygen, it is possible to gasify 8.63 kg oil sludges and obtain 13.63 kg energy gas from the specified composition.

5. Conclusions

The new technology for the gasification of oil wastes is proposed and implemented on the laboratory scale. According to the analyses and measurements, the three types of oil waste studied, namely, GOS, TOS, and petcoke, are mixtures of branched aliphatic hydrocarbons with small contents of aromatic hydrocarbons, contain a large amount of carbon (77–85 wt.%) and sulfur (2.1–3.5 wt.%), and they exhibit a high calorific value of 28–41 MJ/kg.

The technology potentially allows the complete processing of such feedstocks into useful products without emissions into the atmosphere and water bodies and without using special structural materials. These benefits of the technology are based on theoretical studies and laboratory-scale experiments. Theoretically, the gasification products in presumably perfect experimental conditions must contain only CO, H_2, and CO_2 with no hazardous tar (condensable hydrocarbons higher than C_6) and char (mainly solid carbon). In fact, our experiments prove that the dry off-gas contains mostly CO, H_2, and CO_2, but with some CH_4 (up to 10 vol.%) and some small amounts of C_2–C_3 hydrocarbons. Most important is that the gas-phase chromatography implemented with three different devices (Chromatec-Crystal 2000 and GC-MS Chromatec-Crystal 5000 gas chromatographs and MRU VARIO flow gas analyzer) did not show any C_4 and C_5 hydrocarbons. This indirectly means that the dry off-gas does not contain hazardous tar: higher hydrocarbons (C_6 and higher) are generally less thermally stable than the lower hydrocarbons C_1–C_5. As for the char, our experiments definitely show that the carbon content in the ash is caused solely by the shortage of feedstock residence time in the flow-through reactor: The gasification process is accompanied by the removal of mass from the gasifier in the form of fine (1-μm in size) solid ash particles. The same relates to sulfur. The increase in the residence time will surely increase both the carbon and sulfur conversion efficiency: for carbon this was proved experimentally by introducing the helical tube insert between the PDG and the gasifier. The means that increasing the feedstock residence time in the reactor will be studied in the nearest future.

It is also worth mentioning that the technology under consideration is an emerging technology: it is only under development and has been demonstrated only at the laboratory scale so far. The maximum gasification time in our laboratory-scale experiments is about 10–12 min, and the maximum mass of the treated feedstock is generally less than 2 kg. The high concentrations of hydrogen in the off-gas suggest that the sulfur present in the waste reacts with the hydrogen, forming hydrogen sulfide H_2S, which produces a weak aqueous solution of hydrogen sulfide acid with aqueous condensate. In practice, this acid can be concentrated and used as a commercial product. Under our conditions, it was difficult to collect a sufficient amount of condensate from the cyclone and measure the trace amounts of H_2S in the condensate. In the future, we are planning to prove the formation of H_2S acid by direct measurements of the H_2S in the condensate using liquid chromatography in a larger-scale installation.

Author Contributions: Conceptualization, S.M.F.; methodology, S.M.F. and V.A.S.; software, V.A.S.; validation, V.A.S. and F.S.F.; formal analysis, S.M.F., V.A.S. and F.S.F.; investigation, V.A.S., I.A.S., A.S.S., J.K.H., A.G.B., R.U.T., T.V.D., V.G.B., A.B.V., A.V.I. and J.O.I.; resources, S.M.F. and V.Y.P.; data curation, V.A.S., I.A.S., A.S.S., F.S.F., J.K.H., A.G.B., R.U.T., T.V.D., V.G.B., A.V.I. and J.O.I.; writing—original draft preparation, S.M.F.; writing—review and editing, S.M.F.; supervision, S.M.F. and V.Y.P.; project administration, S.M.F. and V.Y.P.; funding acquisition, S.M.F. All authors have read and agreed to the published version of the manuscript.

Funding: This research was partly funded by the Ministry of Science and Higher Education of the Russian Federation, Agreement No. 075-15-2024-543 dated 24 April 2024.

Institutional Review Board Statement: This study does not require ethical approval.

Informed Consent Statement: Not applicable.

Data Availability Statement: The data will be available on request.

Conflicts of Interest: The authors declare no conflicts of interest.

Appendix A. Brief Description of Analytical Methods

Appendix A.1. Express Gravimetry Method

The presence of carbon and hydrogen is determined by express gravimetry [61]. The method is based on the pyrolytic combustion of a substance sample of 3–5 mg in a quartz tube in a flow of oxygen at a temperature of 1248 K in a platinum boat in the presence of PbO. When a sample is burned, CO_2, H_2O, and noncombustible residue are formed. The CO_2 and H_2O are absorbed outside the tube by ascarite and anhydrone, respectively. The C and H contents are calculated by the weight gain of the absorption apparatus, and the percentage of noncombustible residue is calculated by the weight of the ash residue in a quartz test tube. The method error is 0.30–0.50% abs.

Appendix A.2. Dumas–Pregl–Korshun Method

The nitrogen content is determined by the Dumas–Pregl–Korshun method [61]. The method is based on the combustion of a substance sample of 9–10 mg in a quartz glass on a solid oxidizer (granulated nickel oxide II) in a CO_2 atmosphere. The volume of released nitrogen is determined in a nitrogen meter and then the nitrogen content is calculated. The method error is 0.30–0.50% abs.

Appendix A.3. Visual Titration Method

The sulfur content is determined by visual titration [61]. A sample weighed 3–10 mg is burned in a Schöniger flask; 5 mL of water and 10 drops of a 30% hydrogen peroxide solution are used as an absorption medium. Titration is carried out with a 0.04 M solution

of $Ba(CH_3COO)_2$ in the presence of an indicator solution—chlorophosphonazo III. The method error is 0.30–0.50% abs.

Appendix A.4. IR Spectroscopy

The Fourier transform infrared (FTIR) spectra of the substance samples are recorded on an IRTracer-100 FTIR spectrometer (Shimadzu, Japan) using the KBr pellet pressing method. The measurements are recorded in the wavenumber range 4000–450 cm^{-1}.

Appendix A.5. NMR Spectroscopy

NMR spectra are recorded on a Varian INOVA 400 spectrometer (USA), operating at 400 MHz for ^1H and 79 MHz for ^{13}C. The spectra are recorded in carbon tetrachloride as a solvent and processed using MestReNova LITE 8.0 software.

Appendix A.6. Bomb Calorimetry Method

The HHV is measured by the combustion bomb calorimetry method. The amount of heat released during the complete combustion of a sample in a calorimetric bomb in a compressed oxygen environment is measured; the water in the final products remains in a gas state.

The measurements are made using a variable temperature calorimeter ABK-1V (Russia), in which the measure of the amount of heat is the change in the temperature of the calorimetric vessel. When a sample is burned in a bomb, nitric and sulfuric acids form and dissolve in water. According to ref. [62], the correction for nitrogen is determined by titrating the bomb wash with a sodium hydroxide solution with a concentration of 0.1 mol/dm^3. Sulfur analysis is not performed. Tables A1 and A2 show the complete data obtained for the samples of all the studied oil wastes (Table A1) as well as their ash residues (Table A2).

Table A1. Properties of original oil wastes.

Oil Waste	*m*, g	*Q*, J	Q_{sp} J/g	Titr, cm^3	Q_{HNO_3}, J	m_a, g	m_a, %	Q_S, MJ/kg	Δ, %
GOS	0.786410	21,649	27,529	14.4	83	0.0298	3.8	27.4	0.8
GOS	0.945840	26,258	27,762	18.0	104	0.03849	4.9	27.6	
TOS	0.991160	40,195	40,554	21.4	124	0.01836	1.8	40.4	2.0
TOS	0.903380	37,387	41,386	20.0	116	0.01565	1.7	41.3	
petcoke	0.95024	34,606	36,418	30.8	179	0.00902	0.95	36.23	0.06
petcoke	1.000315	36,407	36,396	32.7	190	0.0086	0.86	36.21	

Table A2. Properties of ash residues of oil wastes.

Waste	*m*, g	*Q*, J	Q_{sp}, J/g	m_{H_2O}, g (%)	Solid Residue in Crucible, g (%)	Titr, cm^3	Q_{HNO_3}, J	Q_{Sa}, MJ/kg	Q_i, MJ/kg
GOS	0.897360	8250	9193	0.52 (38%)	0.621 (69%)	6.3	36	9.15	7.74
GOS	1.044605	9581	9172	0.635 (61%)	0.620 (59%)	8.1	47	9.13	7.64
TOS	0.474665	15,674	33,021	0.74 (155%)	0.011 (2.3%)	14	81	32.8	29.0
petcoke	0.961800	28,729	29,870	0.81 (84%)	0.100 (10%)	27.8	161	29.7	27.6
petcoke	1.01634	33,580	33,040	0.5 (49%)	0.0339 (3.3%)	21.2	123	32.9	31.7

Here, *m* is the sample mass; *Q* is the amount of heat measured in the experiment minus the calculated heat of ignition and heat of combustion of auxiliary substances; $Q_{sp} = \frac{Q}{m}$ is the specific heat of combustion of a sample in the bomb; Titr is the volume of sodium hydroxide solution used for titration; $Q_{HNO_3} = 5.8 \cdot \text{Titr}$; m_a is the difference between the masses of the crucible before the experiment and the air-dry crucible after the experiment:

$m_a = \left(\frac{m_a}{m}\right)\cdot 100\%$; $Q_S = Q_{sp} - \frac{Q_{HNO_3}}{m}$ is the HHV of the original oil waste; Q_{Sa} is the HHV of the ash residues of the oil waste; $Q_i = Q_S - \frac{2442 m_{H2O}}{m}$ is the LHV; m_{H2O} is the mass of water condensate formed after the sample combustion; and the error $\Delta = \left(\frac{Q_{Si} - Q_{Si+1}}{\frac{Q_{Si} + Q_{Si+1}}{2}}\right)\cdot 100\%$ is defined as the difference in the masses of the bomb before the experiment (with the crucible removed) and the bomb after the experiment (with the crucible removed).

Appendix B. Granulometric Analysis of Ash Residue Particles

Table A3 presents the results of the granulometric analysis of the ash residue particles for the four studied oil wastes, each averaged over three samples. The particles of all the oil wastes are characterized by a monomodal distribution. The ash residue particles of the GOS, TOS, and petcoke are close in size, whereas the ash residue particles of the TOS–petcoke paste (1:1) have a somewhat larger size. The corresponding curves are presented in Figure 11.

Table A3. Granulometric analysis of ash residue particles for four types of oil waste (averaged over three samples).

Oil Waste	d, μm			Span
	d_{90}	d_{50}	d_{10}	$(d_{90} - d_{10})/d_{50}$
GOS	1.1	0.7	0.4	1.00
TOS	1.2	0.7	0.5	1.00
Petcoke	1.2	0.7	0.5	1.00
TOS–Petcoke paste (1:1)	1.7	1.1	0.7	0.91

References

1. Chen, B.; Zhao, L.; Wang, C.; Chen, S.; Wu, X.; Li, Q.; Zuo, Q. The analysis of formation of polymer-containing oily sludge produced during the wastewater treatment in offshore oilfield. *Energy Sci. Eng.* **2018**, *6*, 675–682. [CrossRef]
2. Kriipsalu, M.; Marques, M.; Maastik, A. Characterization of oily sludge from a wastewater treatment plant flocculation-flotation unit in a petroleum refinery and its treatment implications. *J. Mater. Cycles Waste Manag.* **2008**, *10*, 79–86. [CrossRef]
3. Al-Mebayedh, H.; Niu, A.; Lin, C. Petroleum hydrocarbon composition of oily sludge and contaminated soils in a decommissioned oilfield waste pit under desert conditions. *Appl. Sci.* **2022**, *12*, 1355. [CrossRef]
4. Chu, Z.; Li, Y.; Zhang, C.; Fang, Y.; Zhao, J. A review on resource utilization of oil sludge based on pyrolysis and gasification. *J. Environm. Chem. Eng.* **2023**, *11*, 109692. [CrossRef]
5. Chen, C.; Cang, T.; Wibowo, H.; Hantoko, D.; Kanchanatip, E.; Shen, T.; Yan, M. Comprehensive experimental study on supercritical water gasification of oilfield sludge: Effect of operation parameters, and catalysts on the products. *Int. J. Hydrog. Energ.* **2023**, *48*, 25683–25692. [CrossRef]
6. Chu, Z.; Gong, Z.; Wang, Z.; Zhang, H.; Liu, L.; Wu, J.; Wang, J. Experimental study on gasification of oil sludge with steam and its char characteristic. *J. Hazard. Mat.* **2021**, *416*, 125713. [CrossRef]
7. Kim, J.-H.; Oh, J.-I.; Baek, K.; Park, Y.-K.; Zhang, M.; Lee, J.; Kwon, E.E. Thermolysis of crude oil sludge using CO_2 as reactive gas medium. *Energ. Conv. Manag.* **2019**, *186*, 393–400. [CrossRef]
8. Karengin, A.; Poberezhnikov, A.; Vlasov, A. Plasma disposal of oil wastes. In Proceedings of the 7th International Forum on Strategic Technology (IFOST), Tomsk, Russia, 18–21 September 2012. [CrossRef]
9. Cai, X.; Wei, X.; Du, C. Thermal plasma treatment and co-processing of sludge for utilization of energy and material. *Energ. Fuels* **2020**, *34*, 7775–7805. [CrossRef]
10. Liu, Y.; Song, Y.; Zhang, T.; Jiang, Z.; Siyal, A.; Dai, J.; Fu, J.; Zhou, C.; Wang, L.; Li, X. Microwave-assisted pyrolysis of oily sludge from offshore oilfield for recovery of high-quality products. *J. Hazard. Mater.* **2021**, *420*, 126578. [CrossRef] [PubMed]
11. Qinglong, X.; Chen, Z.; Zhou, Y.; Pan, T.; Duan, Y.; Yu, S.; Liang, X.; Wu, Z.; Ji, W.; Nie, Y. Efficient treatment of oily sludge via fast microwave-assisted pyrolysis, followed by thermal plasma vitrification. *Molecules* **2023**, *28*, 4036. [CrossRef] [PubMed]
12. Z'Graggen, A.; Haueter, P.; Maag, G.; Vidal, A.; Romero, M.; Steinfeld, A. Hydrogen production by steam-gasification of petroleum coke using concentrated solar power–III. Reactor experimentation with slurry feeding. *Int. J. Hydrog Energ.* **2007**, *32*, 992–996. [CrossRef]
13. Larsson, A.; Kuba, M.; Berdugo Vilchesa, T.; Seemann, M.; Hofbauer, H.; Thunman, H. Steam gasification of biomass–Typical gas quality and operational strategies derived from industrial-scale plants. *Fuel Process. Technol.* **2021**, *212*, 106609. [CrossRef]

14. Maric, J.; Berdugo Vilches, T.; Pissot, S.; Cañete Vela, I.; Gyllenhammar, M.; Seemann, M. Emissions of dioxins and furans during steam gasification of automotive shredder residue; experiences from the Chalmers 2–4-MW indirect gasifier. *Waste Manag.* **2020**, *102*, 114–121. [CrossRef] [PubMed]
15. Higman, C.; Van der Burgt, M. *Gasification*; Gulf Professional Publishing: Houston, TX, USA, 2003.
16. Rezaiyan, J.; Cheremisinoff, N. *Gasification Technologies, A Primer for Engineers and Scientists*; Taylor & Francis Group LLC: Boca Raton, FL, USA, 2005.
17. Basu, P. *Biomass Gasification and Pyrolysis, Practical Design*; Elsevier: Amsterdam, The Netherlands, 2010.
18. Bain, R.L.; Broer, K. *Gasification*, 1st ed.; JohnWiley & Sons: Hoboken, NJ, USA, 2011.
19. Frolov, S.M. Organic waste gasification: A selective review. *Fuels* **2021**, *2*, 556–651. [CrossRef]
20. Umeki, K.; Yamamoto, K.; Namioka, T.; Yoshikawa, K. High temperature steam-only gasification of woody biomass. *Appl. Energy* **2010**, *87*, 791–798. [CrossRef]
21. Soni, C.G.; Dalai, A.K.; Pugsley, T.; Fonstad, T. Steam gasification of meat and bone meal in a two-stage fixed-bed reactor system. *Asia Pac. J. Chem. Eng.* **2011**, *6*, 71–77. [CrossRef]
22. Portofino, S.; Donatelli, A.; Iovane, P.; Innella, C.; Civita, R.; Martino, M.; Matera, D.A.; Russo, A.; Cornacchia, G.; Galvagno, S. Steam gasification of waste tyre: Influence of process temperature on yield and product composition. *Waste Manag.* **2013**, *33*, 672–678. [CrossRef]
23. Galvagno, S.; Casu, S.; Casciaro, G.; Martino, M.; Russo, A.; Portofino, S. Steam gasification of Refuse-Derived Fuel (RDF): Influence of process temperature on yield and product composition. *Energy Fuel* **2006**, *20*, 2284–2288. [CrossRef]
24. Galvagno, S.; Casciaro, G.; Casu, S.; Martino, M.; Mingazzini, C.; Russo, A.; Portofino, S. Steam gasification of tire waste, poplar, and refuse-derived fuel: A comparative analysis. *Waste Manag.* **2009**, *29*, 678–689. [CrossRef]
25. Huang, Q.; Wang, J.; Qiu, K.; Pan, Z.; Wang, S.; Chi, Y.; Yan, J. Catalytic pyrolysis of petroleum sludge for production of hydrogen-enriched syngas. *Int. J. Hydrog. Enrg.* **2015**, *40*, 16077–16085. [CrossRef]
26. Cheng, S.; Chang, F.; Zhang, F.; Huang, T.; Yoshikawa, K.; Zhang, H. Progress in thermal analysis studies on the pyrolysis process of oil sludge. *Thermochim. Acta* **2018**, *663*, 125–136. [CrossRef]
27. Cheng, L.; Hu, Q.; Zhang, Z.; Zhang, Z.; Wang, L.; Li, B.; Wang, X.; Liu, S.; Hu, Z. Co-gasification behavior and products distribution of wet sewage sludge and corn stalks: Effect and mechanism analysis of self-moisture utilization. *Int. J. Hydrog. Energ.* **2024**, *56*, 717–724. [CrossRef]
28. Hlina, M.; Hrabovsky, M.; Kavka, T.; Konrad, M. Production of high quality syngas from argon/water plasma gasification of biomass and waste. *Waste Manag.* **2014**, *34*, 63–66. [CrossRef]
29. Hrabovsky, M.; Hlina, M.; Kopecky, V.; Maslani, A.; Zivny, O.; Krenek, P.; Hurba, O. Steam plasma treatment of organic substances for hydrogen and syngas production. *Plasma Chem. Plasma Process.* **2017**, *37*, 739–762. [CrossRef]
30. Wang, M.; Mao, M.; Zhang, M.; Wen, G.; Yang, Q.; Su, B.; Ren, Q. Highly efficient treatment of textile dyeing sludge by CO_2 thermal plasma gasification. *Waste Manag.* **2019**, *90*, 29–36. [CrossRef]
31. Shie, J.L.; Tsou, F.J.; Lin, K.L.; Chang, C.Y. Bioenergy and products from thermal pyrolysis of rice straw using plasma torch. *Bioresour. Technol.* **2010**, *101*, 761–768. [CrossRef] [PubMed]
32. Agon, N.; Hrabovsky, M.; Chumak, O.; Hlina, M.; Kopecky, V.; Masláni, A.; Bosmans, A.; Helsen, L.; Skoblja, S.; Van Oost, G. Plasma gasification or refuse derived fuel in a single-stage system using different gasifying agents. *Waste Manag.* **2016**, *47*, 246–255. [CrossRef] [PubMed]
33. Gomez, E.; Rani, D.A.; Cheeseman, C.R.; Deegan, D.; Wise, M.; Boccaccini, A.R. Thermal plasma technology for the treatment of wastes: A critical review. *J. Hazard. Mater.* **2009**, *161*, 614–626. [CrossRef] [PubMed]
34. Fabry, F.; Rehmet, C.; Rohani, V.; Fulcheri, L. Waste gasification by thermal plasma: A review. *Waste Biomass Valorization* **2013**, *4*, 421–439. [CrossRef]
35. Sanlisoy, A.; Carpinlioglu, M.O. A review on plasma gasification for solid waste disposal. *Int. J. Hydrogen Energy* **2017**, *42*, 1361–1365. [CrossRef]
36. Changming, D.; Chao, S.; Gong, X.; Ting, W.; Xiange, W. Plasma methods for metals recovery from metal–containing waste. *Waste Manag.* **2018**, *77*, 373–387. [CrossRef]
37. Munir, M.T.; Mardon, I.; Al-Zuhair, S.; Shawabkeh, A.; Saqib, N.U. Plasma gasification of municipal solid waste for waste-to-value processing. *Renew. Sustain. Energy Rev.* **2019**, *116*, 109461. [CrossRef]
38. Chun, Y.N.; Song, H.G. Microwave-induced carbon-CO_2 gasification for energy conversion. *Energy* **2020**, *190*, 116386. [CrossRef]
39. Frolov, S.M.; Smetanyuk, V.A.; Avdeev, K.A.; Nabatnikov, S.A. Method for Obtaining Highly Overheated Steam and Detonation Steam Generator Device (Options). Patent of Russian Federation No. 2686138, 24 April 2019.
40. Shahabuddin, M.; Alam, M.T.; Krishna, B.B.; Bhaskar, T.; Perkins, G. A review on the production of renewable aviation fuels from the gasification of biomass and residual wastes. *Bioresour. Technol.* **2020**, *312*, 123596. [CrossRef]
41. Frolov, S.M.; Smetanyuk, V.A.; Sadykov, I.A.; Silantiev, A.S.; Shamshin, I.O.; Aksenov, V.S.; Avdeev, K.A.; Frolov, F.S. Natural gas conversion and liquid/solid organic waste gasification by ultra-superheated steam. *Energies* **2022**, *15*, 3616. [CrossRef]

42. Frolov, S.M. Organic waste gasification by ultra-superheated steam. *Energies* **2023**, *16*, 219. [CrossRef]
43. Frolov, S.M.; Smetanyuk, V.A.; Sergeev, S.S. Reactor for waste gasification with highly superheated steam. *Doklady Phys. Chem.* **2020**, *495*, 191–195. [CrossRef]
44. Frolov, S.M.; Panin, K.S.; Smetanyuk, V.A. Gasification of liquid hydrocarbon waste by the ultra-superheated mixture of steam and carbon dioxide: A thermodynamic study. *Energies* **2024**, *17*, 2126. [CrossRef]
45. Gonzalez, A.M.; Lora, E.E.S.; Palacio, J.C.E.; del Olmo, O.A.A. Hydrogen production from oil sludge gasification/biomass mixtures and potential use in hydrotreatment processes. *Int. J. Hydr. Energ.* **2018**, *43*, 7808–7822. [CrossRef]
46. Kostowski, W.; Tanczuk, M.; Majchrzyk, M.; Banasik, A.; Klimanek, A. Generation of renewable hydrogen from sewage sludge d Quantitative and energy-based technology evaluation. *Int. J. Hydrog. Energ.* **2024**, *52*, 983–994. [CrossRef]
47. Marchetti, L.; Guastaferro, M.; Annunzi, F.; Tognotti, L.; Nicolella, C.; Vaccari, M. Two-stage thermal pyrolysis of plastic solid waste: Set-up and operative conditions investigation for gaseous fuel production. *Waste Manag.* **2024**, *179*, 77–86. [CrossRef] [PubMed]
48. Distaso, E.; Amirante, R.; Calò, G.; De Palma, P.; Tamburrano, P.; Reitz, R.D. Predicting lubricant oil induced pre-ignition phenomena in modern gasoline engines: The reduced GasLube reaction mechanism. *Fuel* **2020**, *281*, 118709. [CrossRef]
49. SDToolBox–Numerical Tools for Shock and Detonation Wave Modeling. Available online: https://shepherd.caltech.edu/SDT (accessed on 12 February 2025).
50. Goodwin, D.G.; Moffat, H.K.; Schoegl, I.; Speth, R.L.; Weber, B.W. Cantera: An Object-Oriented Software Toolkit for Chemical Kinetics, Thermodynamics, and Transport Processes. 2023, Version 3.0.0. Available online: https://zenodo.org/records/8137090 (accessed on 12 February 2025).
51. Byrdin, K.A.; Frolov, S.M.; Storozhenko, P.A.; Guseinov, S.L. Thermochemical study of the detonation properties of boron- and aluminum-containing compounds in air and water. *Shock Waves* **2023**, *33*, 501–520. [CrossRef]
52. Brunauer, S.; Emmett, P.H.; Teller, E. Adsorption of gases in multimolecular layers. *J. Am. Chem. Soc.* **1938**, *60*, 309–319. [CrossRef]
53. Barret, E.P.; Joyner, L.C.; Halenda, P.P. The determination of pore volume and area distributions in porous substances. I. Computations from nitrogen isotherms. *J. Am. Chem. Soc.* **1951**, *73*, 373–380. [CrossRef]
54. Chaiwatanodom, P.; Vivapatarakij, S.; Assabumrungrat, S. Thermodynamic analysis of biomass gasification with CO_2 recycle for synthesis gas production. *Appl. Energy* **2014**, *114*, 10–17. [CrossRef]
55. Di Carlo, A.; Savuto, E.; Foscolo, P.U.; Papa, A.A.; Tacconi, A.; Del Zotto, L.; Aydin, B.; Bocci, E. Preliminary results of biomass gasification obtained at pilot scale with an innovative 100 kWth dual bubbling fluidized bed gasifier. *Energies* **2022**, *15*, 4369. [CrossRef]
56. Tijmensen, M.J.A.; Faaij, A.P.C.; Hamelinck, C.N.; van Hardeveld, M.R.M. Exploration of the possibilities for production of Fischer Tropsch liquids and power via biomass gasification. *Biomass Bioenergy* **2002**, *23*, 129–152. [CrossRef]
57. Nipattummakul, N.; Ahmed, I.; Kerdsuwan, S.; Gupta, A.K. Steam gasification of oil palm trunk waste for clean syngas production. *Appl. Energy* **2012**, *92*, 778–782. [CrossRef]
58. Renganathan, T.; Yadav, M.V.; Pushpavanam, S.; Voolapalli, R.K.; Cho, Y.S. CO_2 utilization for gasification of carbonaceous feedstocks: A thermodynamic analysis. *Chem. Eng. Sci.* **2012**, *83*, 159–170. [CrossRef]
59. Dascomb, J.; Krothapalli, A.; Fakhrai, R. Thermal conversion efficiency of producing hydrogen enriched syngas from biomass steam gasification. *Int. J. Hydrogen Energy* **2013**, *38*, 11790–11798. [CrossRef]
60. Fremaux, S.; Beheshti, S.M.; Ghassemi, H.; Shahsavan-Markadeh, R. An experimental study on hydrogen rich gas production via steam gasification of biomass in a research scale fluidized bed. *Energy Convers. Manag.* **2015**, *91*, 427–432. [CrossRef]
61. Gelman, N.E.; Terentyeva, E.A.; Shanina, G.M.; Kiparenko, L.M.; Rezl, V. *Methods of Quantitative Organic Elemental Microanalysis*; Chemistry Publ.: Moscow, Russia, 1987.
62. *ISO 1928:2009*; Solid Mineral Fuels–Determination of Gross Calorific Value by the Bomb Calorimetric Method and Calculation of Net Calorific Value. ISO: Geneva, Switzerland, 2009. Available online: https://www.iso.org/standard/41592.html (accessed on 12 February 2025).

Disclaimer/Publisher's Note: The statements, opinions and data contained in all publications are solely those of the individual author(s) and contributor(s) and not of MDPI and/or the editor(s). MDPI and/or the editor(s) disclaim responsibility for any injury to people or property resulting from any ideas, methods, instructions or products referred to in the content.